European Network of Fourier-Transform Ion-Cyclotron-Resonance Mass Spectrometry Centers

Grant Agreement n° 731077

Deliverable D4.5 Recommendations to expand harmonics detection to high magnetic field

Start date of the project: 1st January 2018
Duration: 60 months
Project Coordinator: Christian ROLANDO – CNRS-
Contact: christian.rolando@univ-lille.fr

"This project has received funding from the European Union's Horizon 2020 research and innovation programme under grant agreement No 731077"

Document Classification

Title	Recommendations to expand harmonics detection to high magnetic field
Authors	P1 CNRS – Christian Rolando
Work package	WP4 - JRA - Joint Research Actions
Dissemination	PU = Public
Nature	R: Document, report
Doc ID Code	20231102_EU_FT-ICR_MS_D4.5
Keywords	Harmonics detection; High magnetic field; Innovative developments; FT-ICR MS; Quadrupolar detection; Cyclotron frequency; 2ω detection; 7 Tesla instruments; 12 T; 15 T

Document History

Name	Date	Comment
P1 CNRS – Christian Rolando	2023-09-31	

Document Validation

Project Coordinator	Date	E-mail
P1a CNRS-Université de Lille – Christian Rolando	2023-11-01	christian.rolando@univ-lille.fr

Neutral Reviewer	Date	E-mail
P1c CNRS-Université de Rouen – Carlos Afonso	2023-11-01	

Document Abstract

The deliverable D4.5 Recommendations to expand harmonics detection to high magnetic field is a part of the WP4 JRA - Joint Research Actions Task 4.4: Innovative developments in FT-ICR MS, Action c. Exploiting the power of harmonics' detection.

Briefly in FTICR the resolution is proportional to the magnetic field and the acquisition duration. By implementing a quadrupolar detection at two time the cyclotron frequency (2ω detection) allows to double the resolution at constant magnetic field and acquisition duration. The Bruker company has introduced 2ω detection for 7 Tesla instruments recently. In order to exploit the power of the detection of harmonics also for higher magnetic fields the newly introduced 2ω detection technique has been implemented on 12 T and 15 T FT-ICR MS. This deliverable presents the results obtained in the frame of the EU_FT-ICR_MS project.

Table of Contents

1. Introduction

The deliverable D4.5 Recommendations to expand harmonics detection to high magnetic field is a part of the WP4 JRA - Joint Research Actions Task 4.4: Innovative developments in FT-ICR MS, Action c. Exploiting the power of harmonics' detection.

Briefly in FTICR the resolution is proportional to the magnetic field and the acquisition duration. By implementing a quadrupolar detection at two time the cyclotron frequency (2ω detection) allows to double the resolution at constant magnetic field and acquisition duration. The Bruker company has introduced 2ω detection for 7 Tesla instruments recently. In order to exploit the power of the harmonics detection also for higher magnetic fields the newly introduced 2ω detection technique has been implemented on 12 T and 15 T FT-ICR MS. This deliverable presents the results obtained in the frame of the EU_FT-ICR_MS project.

2. Implementation of 2ω detection technique on 12 T and 15 T FT-ICR MS at P1c CNRS-University of Rouen, P3-Czech Academy of Science and P9-University of Warwick

Following the pioneering work of Pr. Evgeny Nikolaev, P8-Skolkovo Institute of Science and Technology, Moscow (see Nikolaev, E. N., Jertz, R., Grigoryev, A., & Baykut, G. (2012). Fine structure in isotopic peak distributions measured using a dynamically harmonized Fourier transform ion cyclotron resonance cell at 7 T. Analytical chemistry, 84(5), 2275-2283.) the Bruker company which is the manufacturer of all the FT-ICR MS of the network introduced in 2018 the SciMax Magnetic Resonance Instrument (MRMS) with 2ω detection. In the EU_EU_FT-ICR proposal we planned to investigate the 2ω detection technique at higher field 12 T and 15 T FT-ICR MS. Initially the Bruker company was part of the EU_EU_FT-ICR proposal and was engaged to afford two prototypes. For legal reasons the Bruker company didn't sign the consortium agreement and withdrew from the EU_EU_FT-ICR consortium. Nevertheless, an agreement was fund with the Bruker company and Bruker agreed to install two 2ω detection prototypes at P1c CNRS-University of Rouen, P3-Czech Academy of Science sites. The development of the prototypes took more time than expected and they were ready and installed only mid-2022. A thirds protype was installed at P9-University of Warwick. The 2 papers in the following chapters from P3-Czech Academy of Science and P9-University of Warwick described the first results obtained with these prototypes.

3. Comparison between an Infinity ICR Cell, a Dynamically Harmonized ICR Cell and a Dynamically Harmonized ICR Cell with quadrupolar detection

3.1 Summary

The fine structure of isotopic peak distributions of glutathione in mass spectra is measured using Fourier transform ion cyclotron resonance mass spectrometry (FT-ICR MS) at 12 and 15 T magnetic field, with an infinity cell and a dynamically harmonized cell (DHC) respectively. The resolved peaks in the fine structure of glutathione consist of 2H, 13C, 15N, 17O, 18O, 33S, 34S, 36S, and combinations of them. The positions of the measured fine structure peaks agree with the simulated isotopic distributions with the mass error less than 250 ppb in broadband mode for the infinity cell and no more than 125 ppb with the DHC after internal calibration. The 15 T FT-ICR MS with DHC cell also resolved around 30 isotopic peaks in broadband with a resolving power (RP) of 2 M. In narrowband (m/z 307−313), our current highest RP of 13.9 M in magnitude mode was observed with

a 36 s transient length by the 15 T FT-ICR MS with the DHC and 2ω detection on the 15 T offers slightly higher RP (14.8 M) in only 18 s. For the 12 T FT-ICR MS with the infinity cell, the highest RP achieved was 15.6 M in magnitude mode with a transient length of 45 s. Peak decay was observed for low abundance peaks, which could be due to the suppression effects from the most abundant peak, as result of ion cloud Coulombic interactions (space-charge). The highest RP observed so far was obtained for the monoisotopic peak of glutathione in narrowband (m/z 307−313) by 15 T FT-ICR MS with 2ω detection. It achieves an RP of 14.8 M within 18 s, which is only half of the acquisition time in 1ω detection (36 s).

3.2 Xu, J., Li, M., Marzullo, B., Wootton, C. A., Barrow, M. P., & O'Connor, P. B. (2022). Fine Structure in Isotopic Peak Distributions Measured Using Fourier Transform Ion Cyclotron Resonance Mass Spectrometry: A Comparison between an Infinity ICR Cell and a Dynamically Harmonized ICR Cell. Journal of the American Society for Mass Spectrometry, 33(8), 1499-1509. https://doi.org/10.1021/jasms.2c00093.

See the pdf of this paper at the end of the deliverable D4.5

4. 2D FTICR MS with 2ω detection

4.1 Summary

Two-dimensional mass spectrometry (2D MS) is a multiplexed tandem mass spectrometry method that does not rely on ion isolation to correlate the precursor and fragment ions. On a Fourier transform ion cyclotron resonance mass spectrometer (FT-ICR MS), 2D MS instead uses the modulation of precursor ion radii inside the ICR cell before fragmentation and yields 2D mass spectra that show the fragmentation patterns of all the analytes. In this study, we perform 2D MS for the first time with quadrupolar detection in a dynamically harmonized ICR cell. We discuss the advantages of quadrupolar detection in 2D MS and how we adapted existing data processing techniques for accurate frequency-to-mass conversion. We apply 2D MS with quadrupolar detection to the top-down analysis of covalently labeled ubiquitin with ECD fragmentation, and we develop a workflow for label-free relative quantification of biomolecule isoforms in 2D MS.

4.2 Polák, M., Palasser, M., Kádek, A., Kavan, D., Wootton, C. A., Delsuc, M. A., ... & van Agthoven, M. A. (2023). Top-Down Proteoform Analysis by 2D MS with Quadrupolar Detection. Analytical Chemistry. In press, https://doi.org/10.1021/acs.analchem.3c02225.

See the pdf of this paper at the end of the deliverable D4.5

5. Conclusion and perspectives

The implementation of 2ω detection prototypes on 12 T and 15 T FT-ICR MS was very successful as it is proved by the already published papers only one year after the prototypes were delivered. The 2ω detection will be implemented as a standard on all the Bruker instruments whatever the magnetic field of the magnet.

ACS Partner Journal

Journal of the American Society for Mass Spectrometry

pubs.acs.org/jasms

Research Article

Fine Structure in Isotopic Peak Distributions Measured Using Fourier Transform Ion Cyclotron Resonance Mass Spectrometry: A Comparison between an Infinity ICR Cell and a Dynamically Harmonized ICR Cell

Jingsha Xu, Meng Li, Bryan Marzullo, Christopher A. Wootton, Mark P. Barrow, and Peter B. O'Connor*

Cite This: *J. Am. Soc. Mass Spectrom.* 2022, 33, 1499−1509

Read Online

ACCESS | Metrics & More | Article Recommendations | Supporting Information

ABSTRACT: The fine structure of isotopic peak distributions of glutathione in mass spectra is measured using Fourier transform ion cyclotron resonance mass spectrometry (FT-ICR MS) at 12 and 15 T magnetic field, with an infinity cell and a dynamically harmonized cell (DHC) respectively. The resolved peaks in the fine structure of glutathione consist of ^{2}H, ^{13}C, ^{15}N, ^{17}O, ^{18}O, ^{33}S, ^{34}S, ^{36}S, and combinations of them. The positions of the measured fine structure peaks agree with the simulated isotopic distributions with the mass error less than 250 ppb in broadband mode for the infinity cell and no more than 125 ppb with the DHC after internal calibration. The 15 T FT-ICR MS with DHC cell also resolved around 30 isotopic peaks in broadband with a resolving power (RP) of 2 M. In narrowband (m/z 307−313), our current highest RP of 13.9 M in magnitude mode was observed with a 36 s transient length by the 15 T FT-ICR MS with the DHC and 2ω detection on the 15 T offers slightly higher RP (14.8 M) in only 18 s. For the 12 T FT-ICR MS with the infinity cell, the highest RP achieved was 15.6 M in magnitude mode with a transient length of 45 s. Peak decay was observed for low abundance peaks, which could be due to the suppression effects from the most abundant peak, as result of ion cloud Coulombic interactions (space-charge).

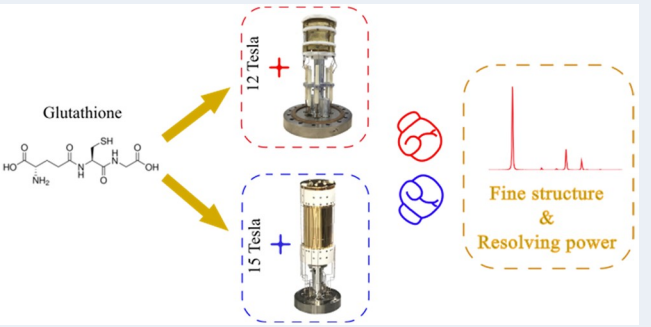

1. INTRODUCTION

In a mass spectrum, the isotopic fine structure of a molecule is defined as the well-resolved individual peaks of this molecule representing every isotopologue.[1] It covers all isotopic combinations of atoms in the molecule. The observation of isotopic fine structure can provide precise assignment of an unknown molecular formula from a complex mass spectrum.[2] Main atoms of organic compounds include carbon, hydrogen, oxygen, nitrogen, sulfur, phosphorus, etc. Among them, isotopes such as ^{12}C, ^{1}H, ^{16}O, and ^{14}N are referred to as the main isotopes. They have approximately 99% or even higher abundance, and ^{32}S has around 95% abundance.[3] Except for phosphorus, each of these elements has additional, lower abundance heavy isotopes such as ^{13}C, ^{17}O, ^{15}N, etc., each of which has a slight mass shift due to the differences in nuclear binding energies, which results in multiple isotopologue peaks for most of the isotopic peaks of most molecules. Isotopologues are molecules which share the same chemical formula and bonding arrangement of atoms but differ only in their isotopic composition, with at least one atom having a different number of neutrons than the parent. When the size of a molecule (increasing the number of atoms) is increased, it becomes more difficult to separate all isotopologues, as the isotopic peaks become more densely distributed due to geometrically increasing combinations of isotopic compositions. For closely spaced peaks, the isotopologues can coalesce into a single peak because of insufficient resolving power (RP). Generally, a m/z 1000 molecule requires a RP at full width half-maximum (fwhm, $m/\Delta m_{50\%}$) of 1−5 M depending on the elemental composition.[1] In the isotopic fine structure of most small molecules (<~1500 Da), the monoisotopic peak represents the molecule consisting of the main isotopes, which is the highest peak in the mass spectrum. Glutathione ($C_{10}H_{17}N_3O_6S$) is a small molecule with a monoisotopic neutral mass ($^{12}C_{10}{}^{1}H_{17}{}^{14}N_3{}^{16}O_6{}^{32}S$) of 307.083806, the fine structure of which consists of a monoisotopic protonated peak (m/z 308.091083) and isotopic peaks with a large number of

Received: March 31, 2022
Revised: June 1, 2022
Accepted: June 3, 2022
Published: June 28, 2022

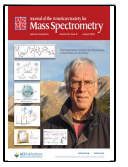

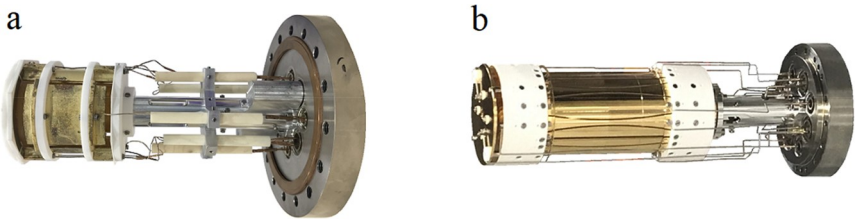

Figure 1. (a) Infinity cell; (b) dynamically harmonized cell (DHC).

combinations of main isotopes and ^{13}C, ^{2}H, ^{15}N, ^{17}O, ^{18}O, ^{33}S, ^{34}S, and ^{36}S.

While it remains challenging for the majority of mass spectrometers to achieve ultrahigh RP, it is routine for Fourier transform ion cyclotron resonance mass spectrometry (FT-ICR MS) to achieve ultrahigh RP and mass accuracy. Modern FT-ICR MS systems at 7 telsa can offer an ultrahigh mass resolving power of 10,000,000.[4] Orbitraps such as Fusion Lumos can also reach a high resolving power of 1 M at m/z 200 with less than 1 ppm mass accuracy.[5,6] At higher magnetic field strength, it is more feasible to resolve the isotopic fine structure,[7] and space charge and cell designs also influence the performance of these instruments to resolve and study such features.

The Infinity ICR cell (Figure 1a) concept is that a closed cylindrical cell with trapping plates at both ends can model the electric excitation field of an infinitely long cell.[8] Linearizing the excitation field in this manner can greatly decrease ion loss along the z-axis compared to the corresponding open-cylindrical cell and, therefore, improve the sensitivity and enable longer transients and higher RP. But it also requires more delicate tuning at high performance. The dynamically harmonized ICR cell (DHC) (commercially marketed as the ParaCell) (Figure 1d) is a novel cell concept.[9] It applies shaped electrodes and inherent trapping motion of the ions to achieve a parabolic trapping potential. The details and electric field of the DHC are described elsewhere.[10] The ParaCell is able to stabilize the cyclotron motion of very low abundance ion clouds, allowing for the measurement of isotopic fine structure and the determination of the molecular formula for a wider dynamic range of ions.[2] It can also stably excite ions to a larger orbit radius than the Infinity Cell, which in turn yields greater signal-to-noise and reduction in space-charge effects.[11] Although not obvious at first glance, the DHC is also much simpler to tune for high performance. The details of the cell geometry designs can be found in a previous study.[12]

In this study, two FTICR MS instruments were applied to investigate the effects of different magnetic fields and the different ICR cell designs on RP and mass accuracy. In addition to the DHC, the 15 T FT-ICR MS is also equipped with 2ω detection. 2ω detection can detect at twice the usual frequency, as four cell plates are used for ion detection instead of the usual two.[13,14] Hence, 2ω detection can significantly improve the instrument performance when other instrument conditions remain the same. Specifically, it can offer the equivalent RP in half of the detection time or double the RP in the same detection time.

2. METHODS

2.1. Chemicals. A 5 μM glutathione solution (L-glutathione reduced, Sigma-Aldrich, Gillingham, UK) was prepared in 50:50 ultrapure water/methanol (VWR Co., Radnor, PA, USA) with 0.1% formic acid (Sigma-Aldrich Company Ltd., Dorset, UK). The standard tuning mix contains different compounds, such as hexamethoxyphosphazene or hexakis(2,2-difluoroethoxy)phosphazene, which gives a clean and evenly distributed mass spectrum of the mass range <3000 Da (Merck, Gillingham, UK). Ultrapure water was obtained from a Millipore Direct-Q purification system (18.2 Ω) (Merck Millipore, MA).

2.2. Instrumentation. The experiments were performed on two Bruker FTICR mass spectrometers (Bruker Daltonik, GmbH, Bremen, Germany) using a custom-built nano-electrospray ionization (nESI) source. One is a 12 T (T) solariX FTICR MS with an infinity cell,[8] and the other is a 15 T solariX 2XR FTICR MS with a dynamically harmonized ICR cell.[9] Singly protonated glutathione ions were generated including the monoisotopic peak (m/z 308.091083), and other isotopic peak clusters were observed in broadband and narrowband (heterodyne mode) spectra and compared with simulated peaks by using the "simulpattern" tool in the DataAnalysis 5.0 software (Bruker Daltonik GmbH). Approximately 10−15 μL of the sample solution was loaded into a glass capillary tip, which was pulled by a P-97 Flaming/Brown micropipette puller (Sutter Instrument Co., Novato, CA), with a nichrome wire inside to provide the electrical connection.[15] Nitrogen at 180 °C was used as the drying gas. A voltage of 600−800 V between the spraying tip and the capillary entrance was applied to facilitate the ESI process. The ions were isolated in the quadrupole mass selector with a m/z range of 20 and then accumulated in the collision cell for 0.08 s prior to transfer to the ICR cell (infinity cell/DHC) for excitation and detection. In both ICR cells (infinity cell & DHC), ions were either excited by a dipolar broadband excitation chirp (frequency sweep from 122 to 1000 Da) or excited and detected in a much narrower m/z range in heterodyne mode. The ion population in the cell was kept high enough to detect the fourth isotopic cluster (m/z 311) but low enough to minimize peak coalescence and ion−ion interactions. Details of the methods' parameters can be found in Tables S1 and S2.

2.3. Data Analysis. All spectra were analyzed using DataAnalysis 5.0 software (Bruker Daltonik GmbH). Internal calibration was carried out to attain subppm assignment uncertainty. The peaks used for internal calibration are the monoisotopic peak and peaks with isotopes of ^{15}N, ^{13}C, ^{34}S, ^{18}O, and $^{13}C^{34}S$. Data processing of 12 T FT-ICR MS used FTMSProcessing 2.2.0 software (Bruker Daltonik GmbH), and data processing of 15 T FT-ICR MS applied FTMSProcessing 2.3.1 software (Bruker Daltonik GmbH). In order to distinguish low-intensity peaks from the sidebands of adjacent high-intensity peaks, a full-sine window function was applied for apodization of the transient, which reduced the original RP by around 20−30%. It is reported that the RP can be doubled when the raw magnitude mode data is "phased" to produce absorption-mode data.[16−18] However, in this work, only

https://doi.org/10.1021/jasms.2c00093
J. Am. Soc. Mass Spectrom. 2022, 33, 1499−1509

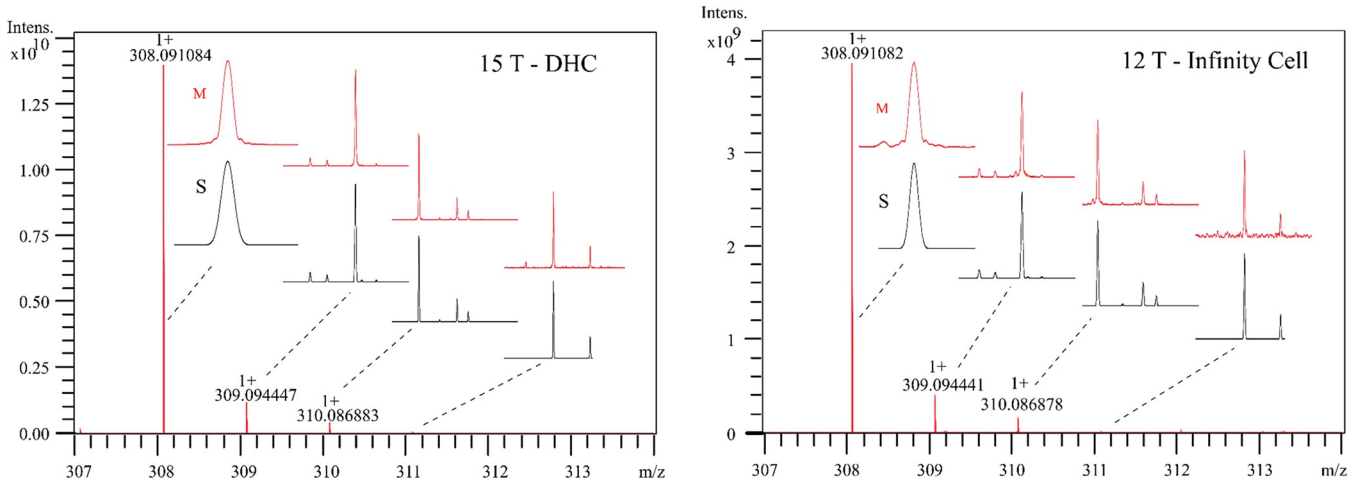

Figure 2. Complete pattern spectra of glutathione acquired in broadband mode using (left) 15 T with a Dynamically Harmonized ICR cell and (right) 12 T with an Infinity ICR cell. Black spectra marked with "S" are the simulated fine structure pattern, and the red spectra marked with "M" are the measured fine structure pattern.

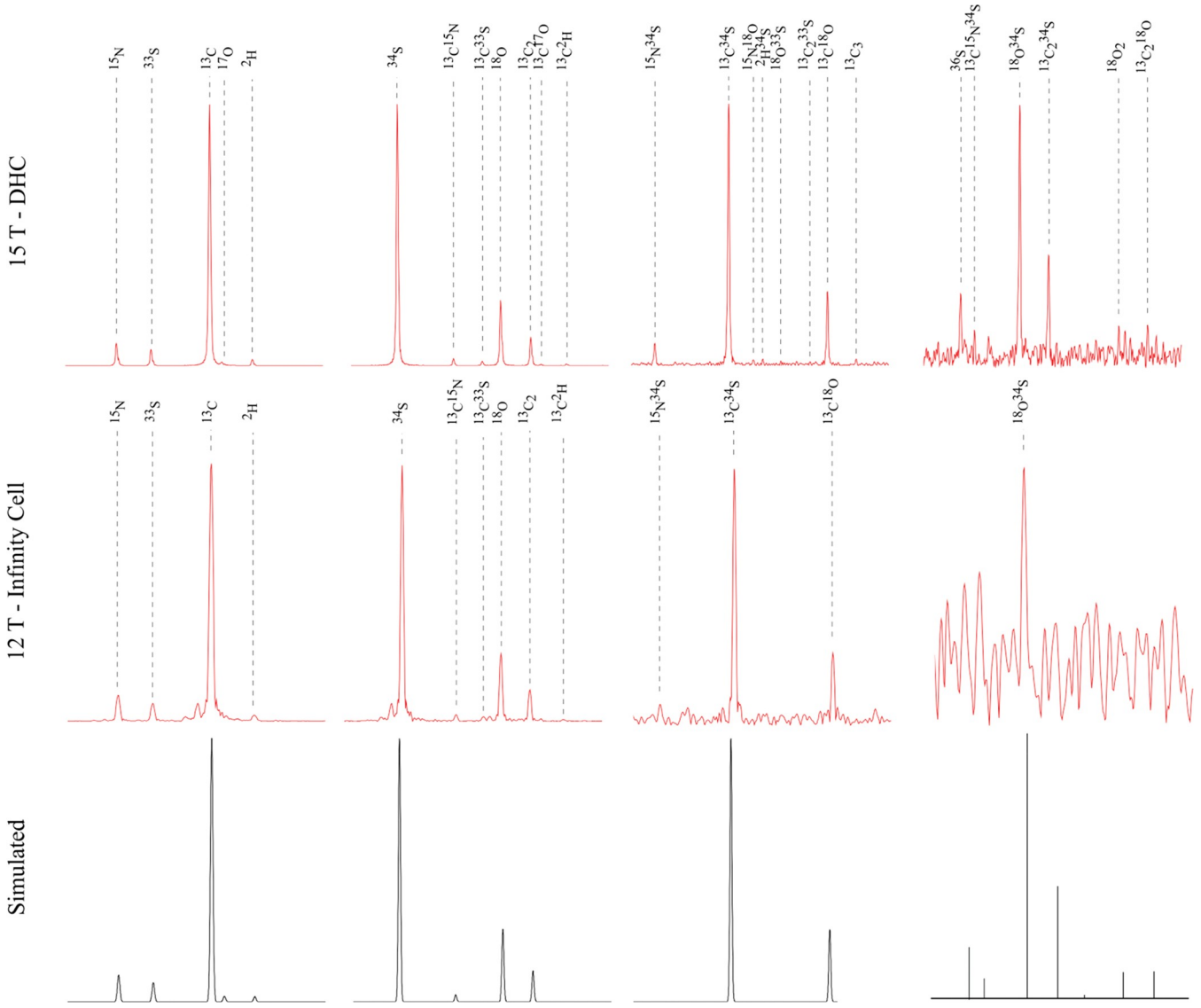

Figure 3. Magnification of the isotopic peak clusters of glutathione.

https://doi.org/10.1021/jasms.2c00093
J. Am. Soc. Mass Spectrom. 2022, 33, 1499−1509

Table 1. m/z and Peak Abundance of the Measured and Simulated Isotopic Fine Structure Spectra of Glutathione with Resolving Powers of 1.96 and 1.00 M for the Monoisotopic Peak Measured by the 15 T with DHC[a] and 12 T with Infinity Cell[b], Respectively, Based on 100 Scans

				15 T-DHC					12 T-infinity cell				
	isotopic peak[c]	theor m/z	theor abundance (%)	measured m/z	measured abundance[d](%)	mass accuracy (ppm)	S/N[e]	rel error of abundance[f] (%)	measured m/z	measured abundance(%)	mass accuracy (ppm)	S/N	rel error of abundance (%)
1		308.091083	100.000	308.091084	100.000	0.0032	110869.2		308.091082	100.000	−0.0032	19519.7	
2	^{15}N	309.088118	1.096	309.088116	0.691	−0.0065	764.4	32.0	309.088119	1.050	0.0032	203.0	3.0
3	^{33}S	309.090471	0.790	309.09047	0.511	−0.0032	565.0	30.3	309.090472	0.716	0.0032	137.7	7.0
4	^{13}C	309.094438	10.816	309.094447	8.665	0.0291	9604.7	15.6	309.094441	10.262	0.0097	2001.2	3.7
5	^{17}O	309.095300	0.229	309.095273	0.116	−0.0874	127.0	46.1					
6	^{2}H	309.097360	0.207	309.097353	0.214	−0.0226	234.7	2.2	309.097359	0.249	−0.0032	46.6	13.1
7	^{34}S	310.086879	4.474	310.086883	3.097	0.0129	3431.4	25.7	310.086878	4.167	−0.0032	811.4	5.0
8	$^{13}C^{15}N$	310.091473	0.119	310.091472	0.084	−0.0032	90.9	24.6	310.09149	0.112	0.0548	19.8	4.3
9	$^{13}C^{33}S$	310.093825	0.085	310.093833	0.052	0.0258	55.8	33.9	310.093817	0.079	−0.0258	13.4	5.4
10	^{18}O	310.095328	1.233	310.095328	0.800	0.0000	884.9	30.1	310.095323	1.109	−0.0161	214.6	7.5
11	$^{13}C_2$	310.097793	0.526	310.097791	0.346	−0.0064	381.2	29.3	310.097794	0.514	0.0032	98.3	1.7
12	$^{13}C^{17}O$	310.098655	0.025	310.098648	0.016	−0.0226	15.4	32.4					
13	$^{13}C^{2}H$	310.100714	0.022	310.100708	0.021	−0.0193	21.3	3.2	310.100643	0.034	−0.2290	4.7	31.2
14	$^{15}N^{34}S$	311.083914	0.049	311.083918	0.029	0.0129	30.1	36.3	311.083889	0.038	−0.0804	5.3	18.8
15	$^{13}C^{34}S$	311.090234	0.484	311.090234	0.331	0.0000	364.5	26.6	311.090235	0.453	0.0032	86.4	4.7
16	$^{15}N^{18}O$	311.092363	0.014	311.092342	0.008	−0.0675	6.7	39.4					
17	$^{2}H^{34}S$	311.093155	0.009	311.093149	0.009	−0.0193	7.9	0.8					
18	$^{18}O^{33}S$	311.094716	0.010	311.09469	0.006	−0.0836	4.9	32.9					
19	$^{13}C_2{}^{33}S$	311.097180	0.004	311.097189	0.005	0.0289	3.9	20.6					
20	$^{13}C^{18}O$	311.098683	0.000	311.09868	0.104	−0.0096	113.2	17.4	311.098661	0.126	−0.0707	22.7	3.6
21	$^{13}C_3$	311.101147	0.015	311.101131	0.009	−0.0514	7.7	37.1					
22	^{36}S	312.086092	0.011	312.086053	0.011	−0.1250	10.1	0.2					
23	$^{13}C^{15}N^{34}S$	312.087268	0.005	312.087231	0.006	−0.1186	4.2	8.1					
24	$^{18}O^{34}S$	312.091124	0.055	312.091107	0.038	−0.0545	40.0	25.9	312.091159	0.045	0.1121	6.8	13.7
25	$^{13}C_2{}^{34}S$	312.093588	0.024	312.093569	0.016	−0.0609	16.1	26.9					
26	$^{18}O_2$	312.099573	0.006	312.099569	0.006	−0.0128	4.9	3.0					
27	$^{13}C_2{}^{18}O$	312.102038	0.006	312.102031	0.006	−0.0224	5.0	4.3					
Average								22.5					8.7

[a] m/z range: 122.86−1000, data transient length: 4.4739 s, 16 M data points (32-bit). [b] m/z range: 122.84−1000, data transient length: 2.7962 s, 8 M data points (32-bit). [c] The isotope peak refers to each of the measured peaks in Figure 3 at +1 charge state. The corresponding isotopologue of the isotopic peak refers to the following formula $^{12}C_{10}{}^{1}H_{17}{}^{14}N_3{}^{16}O_6{}^{32}S$ with the same number of main atoms being replaced with the isotopes, e.g., the isotopologue of the isotopic peak ^{15}N is $^{12}C_{10}{}^{1}H_{17}{}^{14}N_2{}^{15}N^{16}O_6{}^{32}S$. [d] The measured abundance of the ion species is calculated in reference to the intensity of the largest peak in the fine structure spectrum (the monoisotopic peak) and then expressed in percentages. [e] The signal-to-noise ratio S/N of each peak is calculated as $S/N = S/5\sigma$, where S is the peak height above the peak baseline, and the noise N is determined as 5σ, with statistically 99% of the noise values within this range (5σ). [f] Relative error of abundance is calculated as the standard deviation of the theoretical and measured abundance, and then divided by their average and then expressed in percentages.

https://doi.org/10.1021/jasms.2c00093
J. Am. Soc. Mass Spectrom. 2022, 33, 1499−1509

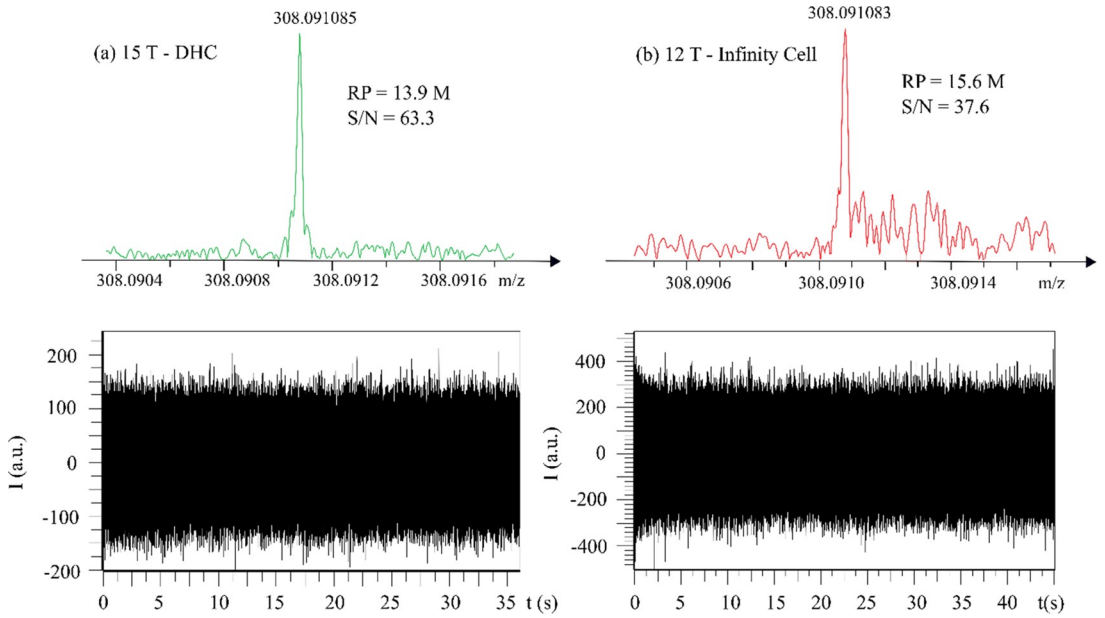

Figure 4. Highest resolving power observed for the monoisotopic peak of glutathione in narrowband (m/z 307−313) by (a) 15 T FT-ICR MS with a dynamically harmonized cell by 1-omega detection and (b) 12 T FT-ICR MS with an infinity cell. (Top) Mass spectra. (Down) Transient signal, single scan data shown.

magnitude-mode data were used for discussion. A phase shift across the spectrum can prevent the absorption mode spectrum from being easily calculated. Hence, the absorption mode needs an accurate phase correction function,[17] but producing an accurate phase function across a narrow m/z range is more difficult than producing the absorption mode spectrum across a full widely spaced spectrum with plenty of real ion (non-noise) peaks.[19] In addition, as the 12 and 15 T instruments are sufficient to split the fine structure of glutathione, and the extra resolving power from using the absorption mode does not result in more information in this particular case.

3. RESULTS AND DISCUSSION

3.1. Broadband Mode. Figure 2 shows the complete fine-structure isotopic pattern spectra of glutathione containing the monoisotopic peak and the first three isotopic peak clusters of protonated glutathione at a RP of 1.96 and 1.00 M measured at the monoisotopic peak on 15 T with DHC (m/z range: 122.86−1000, data transient length: 4.4739 s, 16 M data points (32-bit)) and 12 T with infinity cell (m/z range: 122.84−1000, data transient length: 2.7962 s, 8 M data points (32-bit)), respectively. Figure 3 shows the magnification of the second, third, fourth, and fifth isotopic peak clusters of glutathione, with all peaks labeled with the heavy isotopes—as in Table 1. All m/z values and relative abundances of the clearly observed and resolved isotope peaks are listed in Table 1.

For a given m/z, its corresponding frequency is proportional to the strength of the magnetic field. For example, the corresponding Nyquist frequency of the m/z (122) under 15 T magnetic field is 1875 kHz, while that of the m/z (122) chosen under the 12 T magnetic field is 1500 kHz. As the Nyquist frequency dictates the length of transient for a given number of data points, when the data points are the same for both 15 and 12 T FT-ICR MS, the transient length is inversely proportional to the magnetic field. Based on the calculation of mass resolving power ($m/\Delta m_{50\%}$) under low pressure,[20] to achieve the same RP of a given m/z, the 15 T FT-ICR MS requires 25% less acquisition time compared to the 12 T. When the transient data size of the 15 T experiment is doubled compared to the 12 T in broadband mode, the RP measured at the monoisotopic peak is nearly double that of the 12 T FT-ICR MS.

Figures 2 and 3 show that the positions of the measured fine structure peaks (red) agree with the simulated isotopic distributions (black) for both cells. The A+1, A+2, and A+3 peaks were simulated by the Bruker software "Simulate Isotopic Pattern" with an isotope abundance threshold of 0.1% (default value). The A+4 peaks (line spectra) were simulated using "IsoSpec" with an isotope abundance threshold of 0.001%.[21,22] The 15 T with DHC resolved and observed 12 more isotopic peaks than the 12 T with an infinity cell, which could be partially due to the DHC being better able to stabilize the cyclotron motion of very low abundant ion clouds,[2] and the DHC can also excite ions to a larger stable orbit radius to yield greater signal-to-noise and reduced space-charge effects,[11] as mentioned earlier. The 15 T with the DHC resolved the ^{13}C, $^{13}C_2$, and $^{13}C_3$ peaks, but 12 T with the infinity cell did not resolve the $^{13}C_3$ peak. Peak coalescence was found between the ^{13}C and ^{17}O peaks when the 12 T with infinity cell was used, which could be due to space charge effects or field inhomogeneities within the cell, etc. In Table 1, the mass accuracy/mass error was calculated as the deviation of the measured m/z value and theoretical m/z value of the ion species and then expressed in parts-per-million (ppm). The measured abundance of the ion species is calculated in reference to the intensity of the largest peak in the fine structure spectrum (the monoisotopic peak) and then expressed as a percentage. The relative error of the abundance was calculated as the deviation of the measured and theoretical abundance of the peak and expressed in percentages.

Table 1 shows that the mass errors of the measured and theoretical mass were ≤125 and ≤229 ppb for 15 and 12 T, respectively. The relative error of the measured and theoretical

https://doi.org/10.1021/jasms.2c00093
J. Am. Soc. Mass Spectrom. 2022, 33, 1499−1509

abundance of all peaks ranged between 0.2−46.1% (average: 22.5%) and 1.7−31.2% (average: 8.7%) for 15 and 12 T, respectively. An Orbitrap Exploris 480 mass spectrometer (MS) was applied to successfully resolve the isotopic fine structure at the A+2 peak in the peptide MRFA with isotope abundance accuracies that match the spectral fit. However, this was done with a single selected ion monitoring (SIM) scan with isolation width 50 Th and fixed ion time (IT) of 8 ms, and the mass accuracies of the peaks were mostly between 200 and 600 ppb level.[5] Another Orbitrap Q Exactive Plus mass spectrometer was applied to monitor how different ion populations affect mass and spectral accuracy in different compounds at a resolving power of 140000 at m/z 200. It showed that the Orbitrap slightly underestimates relative abundances of $^{13}C_2$ in caffeine around 12% and $^{34}S_1$ in MRFA around 15%. The relative abundances measured in the Orbitrap ultimately depend on the number of ions injected into the mass analyzer.[23,24] The effects of varying the resolving power were not investigated in the Muddiman study, and the mass accuracies for three compounds were 600−700 ppb.[23] In a paper by Nikolaev et al., the fine structure of isotopic peak clusters in mass spectra of reserpine and substance P were measured using 7 T FT-ICR MS with a DHC.[3] The mass accuracies of the fine structure peaks were ≤200 ppb, which are comparable with this study. Some deviations from the theoretical isotopic distribution were also observed in their study. The peak intensity differences between the measured and theoretical peaks were mostly in the range of 30−70%, which are higher than those peak abundance deviations in this study. In this work, the 15 T showed higher relative abundance error for many of the isotopologues than the 12 T, but the signal/noise value (S/N) of the most abundant peak is also 5.7× higher, suggesting space-charge is contributing to the deviations. However, it is important to note that the two cells are different and also have different preamplifier designs, so the S/N levels may not be directly comparable, but in many cases, the information on mass-to-charge ratio and relative abundance are enough for unambiguous assignment of the elemental formula.[3]

3.2. Narrowband/Heterodyne Mode. *3.2.1. Comparison of Narrowband Data.* Compared with broadband mode, which uses a wide frequency excitation, the advantage of narrowband detection is the increase of data points per frequency, which can result in much longer transient length and higher RP. Figure 4 presents the mass spectra and transient signal in narrowband mode with narrow mass range m/z 307−313 and data size of 1 M by both 15 T FT-ICR MS with a DHC and 12 T FT-ICR MS with an infinity cell. In this study, the recorded longest transient lengths of the 15 and 12 T were 36 and 45 s, respectively, with the corresponding highest RP observed for the monoisotopic peak of glutathione at 13.9 and 15.6 M, respectively. The 50 and 97 s transients were reported previously by a 9.4 T SolariX XR FT-ICR MS with a paracell in heterodyne mode.[25] In this work, longer transient and higher RP can be achieved if the m/z window is set narrower. However, m/z 307−313 was applied here to include all possible isotopic peaks that can be detected by the instruments.

As the effective length and quality of the transient signals are limited by the space charge effects in the ICR cell,[26] for the long transient, it is necessary to keep the ion populations relatively low in the cell to minimize these ion−ion charge-repulsion interaction effects. However, low ion populations will also result in low intensity of the detected ion peaks, which makes it difficult to observe less abundant peaks even with hundreds of accumulated scans. Therefore, for better comparison of fine structure data, the data size of 512 k in narrowband was used. The mass accuracies and measured abundance are summarized in Table 2.

In Table 2, resolving powers of 7.5 M (15 T, transient duration: 18.0355 s) and 7.6 M (12 T, transient duration: 22.5444 s) are observed for the monoisotopic peak measured by the 15 T with DHC and 12T with infinity cell, respectively. The measured mass accuracies/errors were <709 and ≤521 ppb for the 15 T-DHC and 12 T-Infinity cell, respectively, though these mass accuracy values also include some very low intensity peaks which unsurprisingly also have the highest errors due to distortion of peakshapes by the noise, impeding peak analysis. The relative error of the measured and theoretical abundance of all peaks ranged between 2.0−67.9% (average: 23.8%) and 9.4−134.6% (average: 44.4%) on the 15 and 12 T, respectively, and the S/N values are comparable to minimize any differential space-charge effects between the two data sets. To investigate the possible effects of the resolving power on the relative abundance error, we compared the relative abundance of the two most abundant isotopic peaks of glutathione under different size of data points, as other peaks are hard to observe under lower resolving power. As shown in Figure 5, the relative abundance of m/z 309 and 310 are much lower than the theoretical abundance measured by the 12 T, and they approach the theoretical abundance values when the resolving power is decreased, as indicated by reduced data points. For the data obtained from the 15 T with the DHC, the relative abundance of m/z 309 and 310 are closer to the theoretical abundance. The relative abundance approaches the theoretical abundance when the data points are reduced from 1024 to 256 k, while they almost maintained at the theoretical values when the data points were reduced from 256 to 32 k. The data from both broadband and narrowband showed that a higher signal-to-noise ratio is preferable to assign more isotopic peaks. In narrowband, even though the RP is significantly improved, the low S/N leads to fewer assigned peaks than broadband. Therefore, more accumulated scans are needed to accurately assign more peaks. However, this will require delicate tuning of the cell and ions to minimize space-charge frequency shifts, especially during a very long transient. With very high resolution, on any Fourier Transform instrument, including the Orbitrap, signal averaging can be problematic if the peaks are shifting from scan-to-scan slightly due to space-charge frequency shifts.

As shown in Tables 1 and 2, among all measured isotopologues, those with theoretical abundance <1%, such as isotopologues with isotopes ^{17}O, ^{2}H, $^{2}H^{34}S$, and $^{18}O^{33}S$, are observed with much higher mass errors and relative abundance errors. This is possibly due to the small ion clouds in the ICR cell which can be strongly influenced by large ion clouds of similar m/z during the detection period, as these ion clouds are transiting through each other with a frequency equal to the difference of their cyclotron frequencies.[3,27,28] This ion cloud interaction may have affected the relative positions and relative abundance of these peaks in the measured fine structure. In some extreme cases, this ion cloud interaction can cause peak coalescence,[29,30] or totally/partially disperses the small ion cloud's coherence, and lead to the decrease of peak intensity or completely eliminate the low abundance peak. To investigate

https://doi.org/10.1021/jasms.2c00093
J. Am. Soc. Mass Spectrom. 2022, 33, 1499−1509

Table 2. Narrowband Mass and Peak Abundance of the Measured and Simulated Isotopic Fine Structure Spectra of Glutathione with Resolving Powers of 7.5 and 7.6 M for the Monoisotopic Peak Measured by the 15 T with DHC[a] and 12T with Infinity Cell,[b] Respectively, Based on 10 Scans

	isotopic peak	theor m/z	theor abundance (%)	15 T-DHC (1ω) measured m/z	abundance (%)	mass accuracy (ppm)	S/N	rel error of abundance (%)	12 T-infinity cell measured m/z	abundance (%)	mass accuracy (ppm)	S/N	rel error of abundance (%)
1		308.091083	100.000	308.091083	100.000	0.0000	1048.4		308.09108	100.000	−0.0097	1768.5	
2	^{15}N	309.088118	1.096	309.088117	1.013	−0.0032	8.6	5.6	309.088122	0.760	0.0129	11.5	25.6
3	^{33}S	309.090471	0.790	309.090473	1.208	0.0065	10.6	29.6	309.090476	0.635	0.0162	9.3	15.4
4	^{13}C	309.094438	10.816	309.094438	10.512	0.0000	108.1	2.0	309.094438	9.471	0.0000	165.9	9.4
5	^{17}O	309.095300	0.229	309.095519	0.474	0.7085	2.9	49.3	309.095364	0.556	0.2071	7.8	58.9
6	^{2}H	309.097360	0.207	309.097501	0.589	0.4562	4.1	67.9	309.097381	0.376	0.0679	4.7	41.0
7	^{34}S	310.086879	4.474	310.086878	3.739	−0.0032	37.2	12.7	310.086877	3.371	−0.0064	57.7	19.9
8	^{18}O	310.095328	1.233	310.095328	0.951	0.0000	8.0	18.3	310.095321	0.978	−0.0226	15.3	16.3
9	$^{13}C_2$	310.097793	0.526	310.097794	0.619	0.0032	4.5	11.5	310.097806	0.384	0.0419	4.8	22.1
10	$^{13}C^{34}S$	311.090234	0.484	311.090234	0.621	0.0000	4.5	17.5	311.090237	0.571	0.0096	8.1	11.7
11	$^{2}H^{34}S$	311.093155	0.009						311.092993	0.365	−0.5207	4.5	134.6
12	$^{18}O^{33}S$	311.094716	0.010						311.094866	0.347	0.4822	4.2	133.5
avg								23.8					44.4

[a] m/z range: 307−313, data transient length: 18.0355 s, 512 k data points (32-bit). [b] m/z range: 307−313, data transient length: 22.5444 s, 512 k data points (32-bit).

this phenomenon, the three most abundant peaks are chosen and presented below.

3.2.2. Peak Decay. To compare this interaction phenomenon on both instruments, data with similar intensities and acquisition time were selected. The data was acquired in narrow mass range (m/z 307−313) with a data size of 256 k on the 15 T FT-ICR MS, while it was acquired in mass range of (m/z 294−324) with a data size of 1 M on the 12 T FT-ICR MS. The transient length was 9.0177 and 8.808 s for the 15 and 12 T, respectively, which was the most readily available compromise of parameters to provide very similar length transients and thus more comparable conditions. Each transient was divided into 32 equal segments. As it is difficult to observe the small peaks when the transient signal is divided into small segments, Figure 6 only plotted the segmented and accumulated peak intensities of the three most abundant peaks versus the acquisition time. To be more comparable in intensity with the m/z 308 peak, the peak intensities of the most abundant m/z 309 and 310 peaks are increased by 10- and 25-fold, respectively.

As shown in Figure 6a,b, the segment intensity of lower intensity peaks (m/z 309 and 310) decays faster than the higher intensity peak m/z 308 for both instruments. These peaks (m/z 309 and 310) also accumulated more slowly than the large peak m/z 308, as presented in Figure 6 c,d. This is most likely because the ion cloud interactions at the intensities of smaller peaks are generally suppressed by the more intense peak, and the minor ion "packets" are more vulnerable to the increase of any possible space charge interactions.[31] The peaks measured by 12 T decay faster than those of the 15 T in the beginning, which may be due to space charge effects that resulted from insufficiently delicate tuning of the 12 T with an Infinity cell. Generally, to improve the sensitivity, ions are usually detected at ∼50% of the cell radius. However, electric field homogeneity only exists near the center of the infinity cell. Hence, the ions are either confined to small populations at the center of the cell which are subjected to space charge effects or the ions are excited to a larger orbit where the inhomogeneities can result in the loss of coherence.[32] Thus, the infinity cell requires very delicate tuning to prevent coherence loss while maintaining sufficient sensitivity. In the DHC, the homogeneity of the electric field inside the cell allows the ions to be spaced out, which not only reduce the space charge effects but also increase the sensitivity, as the ions have larger orbit radius and closer to the detection plates. The DHC and/or the higher magnetic field may have also helped with preserving lower abundance ion cloud coherence. In addition, unlike the DHC, the center of gyration of the magnetron motion cannot be tuned/minimized via $x-y$ deflection in the infinity cell as it can be in the DHC.

3.3.3. 2-Omega Detection. Apart from a normal dipolar 1-omega (1ω) detection on both 12 and 15 T FT-ICR MS, the DHC on the 15 T FT-ICR MS is also equipped with quadrupolar 2-omega (2ω) detection, which enables equivalent RP in half of the detection time or double the RP in the same detection time when other instrument conditions remain the same.[33] The postcapture delay (PCD) curve was developed by Jertz et al. to study the behavior of the magnetron motion and quality of the centralization of both magnetron and cyclotron motion within the ParaCell by acquiring a series of FT-ICR spectra using varied PCD time intervals.[10] The postcapture delay time refers to the time period that after the capture of the ions in the cell and before the start of cyclotron

https://doi.org/10.1021/jasms.2c00093
J. Am. Soc. Mass Spectrom. 2022, 33, 1499−1509

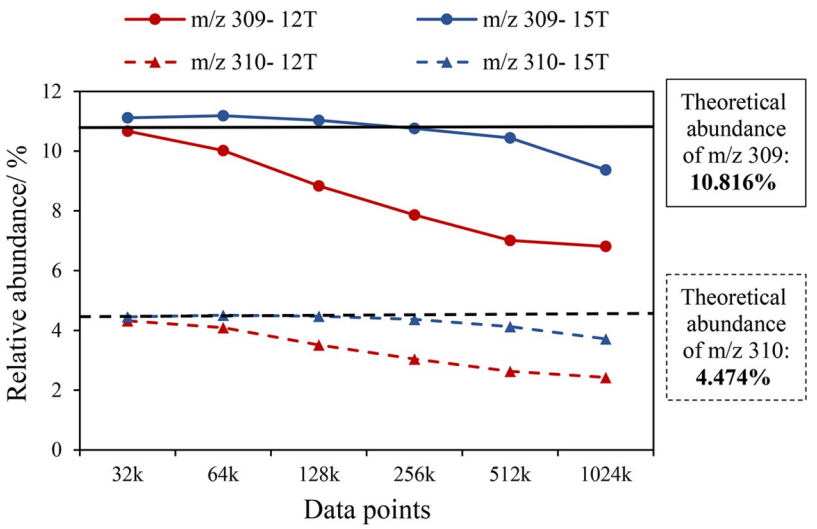

Figure 5. Relative abundance of the two most abundant isotopic peaks of glutathione measured by 12 T FT-ICR MS with an infinity ICR cell and 15 T FT-ICR MS with a dynamically harmonized ICR cell under different size of data points, based on 50 scans.

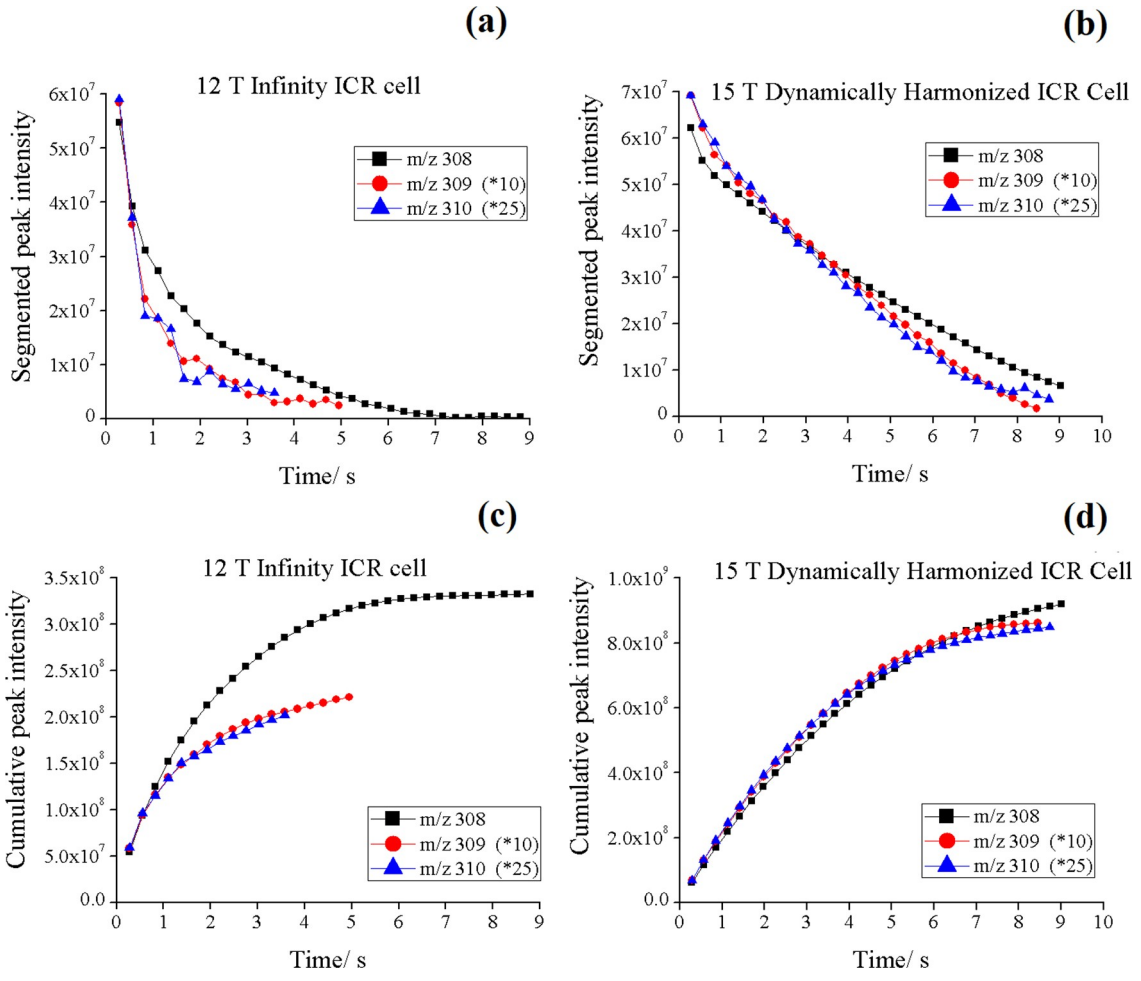

Figure 6. Segmented peak intensities of the three most abundant peaks of glutathione measured by (a) 12 T FT-ICR MS with an infinity ICR cell and (b) 15 T FT-ICR MS with a dynamically harmonized ICR cell; each point represent a segment of 1/32 of the total transient length. Cumulative peak intensities of the three most abundant peaks of glutathione measured by (c) 12 T FT-ICR MS with an infinity ICR cell and (d) 15 T FT-ICR MS with a dynamically harmonized ICR cell.

excitation of the ion. In this study, the delay time varied from 0 to 500 ms with 5 ms steps.

Figure 7 is an example of the postcapture delay (PCD) curve measured by 15 T FT-ICR MS with dynamically harmonized cell in 2ω detection mode. The peak with highest intensity ($m/$

https://doi.org/10.1021/jasms.2c00093
J. Am. Soc. Mass Spectrom. 2022, 33, 1499−1509

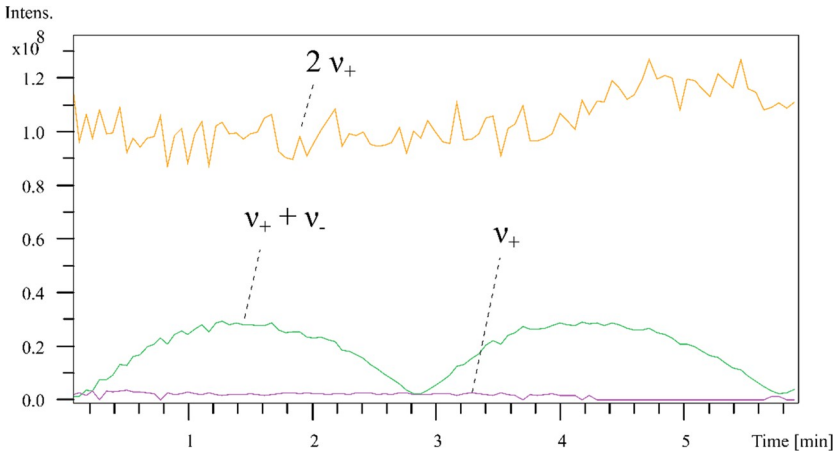

Figure 7. PCD curve measured by 15 T FT-ICR MS with dynamically harmonized cell in 2ω detection mode.

z 922.00968) of the standard tuning mix was chosen as the fundamental mass peak, and the relevant harmonic signals in quadrupolar 2ω detection appear at half of the frequency ν_+ and $\nu_+ + \nu_-$, which is twice of the fundamental mass (ν_+: 249, 828.56 Hz and m/z 1843.98379; $\nu_+ + \nu_-$: 249, 832.46 Hz and m/z 1843.95491) in 2ω mode.[34] The difference between ν_+ and $\nu_+ + \nu_-$ is the magnetron frequency ν_-, which is 3.9 Hz. By plotting the relative intensity of ν_+ and $\nu_+ + \nu_-$ versus the PCD time in each mass spectrum leads to an oscillating "PCD curve". The position and height of minima and maxima of this PCD curve can be used to explain the size and the position of the magnetron orbit. In Figure 7, the 2 ν_+ signal (orange line) represents the intensity variation of the fundamental mass peak under different PCD time. The two signals with frequencies ν_+ and $\nu_+ + \nu_-$ represent the off-axis cyclotron motion and magnetron motion, respectively. As shown in Figure 7, the off-axis cyclotron motion (purple line) is very stable with intensities close to 0. The green line is a stable oscillating curve, representing the magnetron motion under different PCD time intervals. When the PCD time equals to 0, the intensities of the ν_+ and $\nu_+ + \nu_-$ peaks are also close to 0, which suggest an acceptable tuning of the DHC.

Figure 8 exhibited the highest RP observed so far for the monoisotopic peak of glutathione in narrowband (m/z 307−313) by 15 T FT-ICR MS with 2ω detection. It achieves an RP of 14.8 M within 18 s, which is only half of the acquisition time in 1ω detection (36 s).

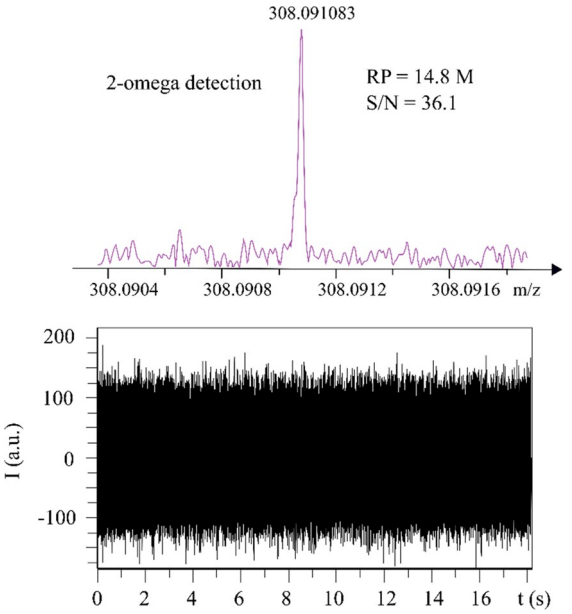

Figure 8. Highest resolving power observed for the monoisotopic peak of glutathione in narrowband (m/z 307−313) by 15 T FT-ICR MS with dynamically harmonized cell in 2ω detection mode. (Top) mass spectra; (down) transient signal, single scan data shown.

4. CONCLUSIONS

The fine structure of isotopic peak distributions of glutathione in mass spectra was measured using Fourier transform ion cyclotron resonance mass spectrometry at 12 and 15 T magnetic field with an Infinity cell and a Dynamically Harmonized Cell, respectively. The positions of the measured fine structure peaks in the broadband agree with the simulated isotopic distributions with the mass error ≤125 and ≤229 ppb for the DHC and infinity cell, respectively. In heterodyne mode with a mass window of 6 m/z, we have shown that the highest RPs that can be achieved by FT-ICR MS are 13.9 and 15.6 M by the 15 T with DHC (transient length: 36 s) and 12 T with infinity cell (transient length: 45 s), respectively. Here, we demonstrated that the 2ω detection offers equivalent RP (14.8 M) in only half of the detection time (18 s). There is noticeable peak decay found for low abundance peaks, which may be the result of the suppression effects by the most abundant peak. The DHC was shown to be able to maintain detection of lower intensity species for a much longer time and with a more consistent decay constant between high and low intensity species than the infinity cell during comparable analysis.

Although this study provides a comparison of the DHC and infinity cell, it should be noted that this is not a direct comparison of two cells as there are other variables which also differ, such as different magnetic field, electronics, method parameters, etc.

■ ASSOCIATED CONTENT

Supporting Information

The Supporting Information is available free of charge at https://pubs.acs.org/doi/10.1021/jasms.2c00093.

Method parameters for the broadband and narrowband data (Tables S1 and S2) (PDF)

https://doi.org/10.1021/jasms.2c00093
J. Am. Soc. Mass Spectrom. 2022, 33, 1499−1509

AUTHOR INFORMATION

Corresponding Author

Peter B. O'Connor − *Department of Chemistry, University of Warwick, Coventry CV4 7AL, United Kingdom*; Phone: +44 (0)24 76151008; Email: p.oconnor@warwick.ac.uk

Authors

Jingsha Xu − *Department of Chemistry, University of Warwick, Coventry CV4 7AL, United Kingdom;* Present Address: Beihang Hangzhou Innovation Institute Yuhang, Xixi Octagon City, Yuhang District, Hangzhou 310023, China

Meng Li − *Department of Chemistry, University of Warwick, Coventry CV4 7AL, United Kingdom*

Bryan Marzullo − *Department of Chemistry, University of Warwick, Coventry CV4 7AL, United Kingdom*

Christopher A. Wootton − *Department of Chemistry, University of Warwick, Coventry CV4 7AL, United Kingdom;* Present Address: Bruker Daltonics GmbH & Co. KG, Bremen, Germany.

Mark P. Barrow − *Department of Chemistry, University of Warwick, Coventry CV4 7AL, United Kingdom;* orcid.org/0000-0002-6474-5357

Complete contact information is available at: https://pubs.acs.org/10.1021/jasms.2c00093

Notes

The authors declare no competing financial interest.

ACKNOWLEDGMENTS

We thank Dr. Diana Catalina Palacio Lozano and Johanna Paris for their assistance in instrument tuning and Hugh Jones, Callan Littlejohn for their assistance in data analysis. This work is funded by EPSRC funding (J003022, N021630, L015307, N033191,V007718), BBSRC funding (P021875, R022399), the H2020 EU- FTICR Network (project 731077), Bruker Daltonics, the University of Warwick, and the Department of Chemistry.

REFERENCES

(1) Wei, J.; Antzutkin, O. N.; Filippov, A. V.; Iuga, D.; Lam, P. Y.; Barrow, M. P.; Dupree, R.; Brown, S. P.; O'Connor, P. B. Amyloid Hydrogen Bonding Polymorphism Evaluated by 15n{17o}Reapdor Solid-State Nmr and Ultra-High Resolution Fourier Transform Ion Cyclotron Resonance Mass Spectrometry. *Biochem.* **2016**, *55* (14), 2065−2068.

(2) Thompson, C. J.; Witt, M.; Forcisi, S.; Moritz, F.; Kessler, N.; Laukien, F. H.; Schmitt-Kopplin, P. An Enhanced Isotopic Fine Structure Method for Exact Mass Analysis in Discovery Metabolomics: Fia-Casi-Ftms. *J. Am. Soc. Mass Spectrom.* **2020**, *31* (10), 2025−2034.

(3) Nikolaev, E. N.; Jertz, R.; Grigoryev, A.; Baykut, G. Fine Structure in Isotopic Peak Distributions Measured Using a Dynamically Harmonized Fourier Transform Ion Cyclotron Resonance Cell at 7 T. *Anal. Chem.* **2012**, *84* (5), 2275−2283.

(4) Ghaste, M.; Mistrik, R.; Shulaev, V. Applications of Fourier Transform Ion Cyclotron Resonance (Ft-Icr) and Orbitrap Based High Resolution Mass Spectrometry in Metabolomics and Lipidomics. *Int. J. Mol. Sci.* **2016**, *17* (6), 816.

(5) Denisov, E.; Damoc, E.; Makarov, A. Exploring Frontiers of Orbitrap Performance for Long Transients. *Int. J. Mass Spectrom.* **2021**, *466*, 116607.

(6) Hoegg, E. D.; Godin, S.; Szpunar, J.; Lobinski, R.; Koppenaal, D. W.; Marcus, R. K. Coupling of an Atmospheric Pressure Microplasma Ionization Source with an Orbitrap Fusion Lumos Tribrid 1m Mass Analyzer for Ultra-High Resolution Isotopic Analysis of Uranium. *J. Anal. At. Spectrom.* **2019**, *34* (7), 1387−1395.

(7) Shi, S. D.-H.; Hendrickson, C. L.; Marshall, A. G. Counting Individual Sulfur Atoms in a Protein by Ultrahigh-Resolution Fourier Transform Ion Cyclotron Resonance Mass Spectrometry: Experimental Resolution of Isotopic Fine Structure in Proteins. *Proc. Natl. Acad. Sci. U.S.A.* **1998**, *95* (20), 11532−11537.

(8) Caravatti, P.; Allemann, M. The 'Infinity Cell': A New Trapped-Ion Cell with Radiofrequency Covered Trapping Electrodes for Fourier Transform Ion Cyclotron Resonance Mass Spectrometry. *Organ. Mass Spectrom.* **1991**, *26* (5), 514−518.

(9) Nikolaev, E. N.; Boldin, I. A.; Jertz, R.; Baykut, G. Initial Experimental Characterization of a New Ultra-High Resolution Fticr Cell with Dynamic Harmonization. *J. Am. Soc. Mass Spectrom.* **2011**, *22* (7), 1125−1133.

(10) Jertz, R.; Friedrich, J.; Kriete, C.; Nikolaev, E. N.; Baykut, G. Tracking the Magnetron Motion in Ft-Icr Mass Spectrometry. *J. Am. Soc. Mass Spectrom.* **2015**, *26* (8), 1349−1366.

(11) Cho, E.; Witt, M.; Hur, M.; Jung, M.-J.; Kim, S. Application of Ft-Icr Ms Equipped with Quadrupole Detection for Analysis of Crude Oil. *Anal. Chem.* **2017**, *89* (22), 12101−12107.

(12) Nikolaev, E.; Lioznov, A. Evaluation of Major Historical Icr Cell Designs Using Electric Field Simulations. *Mass Spectrom. Rev.* **2022**, *41* (2), 262−283.

(13) Thomas, M. J.; Collinge, E.; Witt, M.; Palacio Lozano, D. C.; Vane, C. H.; Moss-Hayes, V.; Barrow, M. P. Petroleomic Depth Profiling of Staten Island Salt Marsh Soil: 2ω Detection Fticr Ms Offers a New Solution for the Analysis of Environmental Contaminants. *Sci. Total Environ.* **2019**, *662*, 852−862.

(14) Nikolaev, E. N.; Gorshkov, M. V.; Mordehai, A. V.; Talrose, V. L. Ion Cyclotron Resonance Signal-Detection at Multiples of the Cyclotron Frequency. *Rapid Commun. Mass Spectrom.* **1990**, *4* (5), 144−146.

(15) Marzullo, B. P.; Morgan, T. E.; Wootton, C. A.; Li, M.; Perry, S. J.; Saeed, M.; Barrow, M. P.; O'Connor, P. B. Comparison of Fragmentation Techniques for the Structural Characterization of Singly Charged Agrochemicals. *Anal. Chem.* **2020**, *92* (4), 3143−3151.

(16) Palacio Lozano, D. C.; Gavard, R.; Arenas-Diaz, J. P.; Thomas, M. J.; Stranz, D. D.; Mejía-Ospino, E.; Guzman, A.; Spencer, S. E. F.; Rossell, D.; Barrow, M. P. Pushing the Analytical Limits: New Insights into Complex Mixtures Using Mass Spectra Segments of Constant Ultrahigh Resolving Power. *Chem. Sci.* **2019**, *10* (29), 6966−6978.

(17) Kilgour, D. P. A.; Wills, R.; Qi, Y.; O'Connor, P. B. Autophaser: An Algorithm for Automated Generation of Absorption Mode Spectra for Ft-Icr Ms. *Anal. Chem.* **2013**, *85* (8), 3903−3911.

(18) Qi, Y.; Li, H.; Wills, R. H.; Perez-Hurtado, P.; Yu, X.; Kilgour, D. P. A.; Barrow, M. P.; Lin, C.; O'Connor, P. B. Absorption-Mode Fourier Transform Mass Spectrometry: The Effects of Apodization and Phasing on Modified Protein Spectra. *J. Am. Soc. Mass Spectrom.* **2013**, *24* (6), 828−834.

(19) Qi, Y.; Thompson, C. J.; Van Orden, S. L.; O'Connor, P. B. Phase Correction of Fourier Transform Ion Cyclotron Resonance Mass Spectra Using Matlab. *J. Am. Soc. Mass Spectrom.* **2011**, *22* (1), 138−147.

(20) Marshall, A. G.; Hendrickson, C. L.; Jackson, G. S. Fourier Transform Ion Cyclotron Resonance Mass Spectrometry: A Primer. *Mass Spectrom. Rev.* **1998**, *17* (1), 1−35.

(21) Łacki, M. K.; Startek, M.; Valkenborg, D.; Gambin, A. Isospec: Hyperfast Fine Structure Calculator. *Anal. Chem.* **2017**, *89* (6), 3272−3277.

(22) Łącki, M. K.; Valkenborg, D.; Startek, M. P. Isospec2: Ultrafast Fine Structure Calculator. *Anal. Chem.* **2020**, *92* (14), 9472−9475.

(23) Khodjaniyazova, S.; Nazari, M.; Garrard, K. P.; Matos, M. P. V.; Jackson, G. P.; Muddiman, D. C. Characterization of the Spectral Accuracy of an Orbitrap Mass Analyzer Using Isotope Ratio Mass Spectrometry. *Anal. Chem.* **2018**, *90* (3), 1897−1906.

(24) Gorshkov, M. V.; Fornelli, L.; Tsybin, Y. O. Observation of Ion Coalescence in Orbitrap Fourier Transform Mass Spectrometry. *Rapid Commun. Mass Spectrom.* **2012**, *26* (15), 1711−1717.
(25) Nagornov, K. O.; Kozhinov, A. N.; Nicol, E.; Tsybin, O. Y.; Touboul, D.; Brunelle, A.; Tsybin, Y. O. Narrow Aperture Detection Electrodes Icr Cell with Quadrupolar Ion Detection for Ft-Icr Ms at the Cyclotron Frequency. *J. Am. Soc. Mass Spectrom.* **2020**, *31* (11), 2258−2269.
(26) Miladinović, S. M.; Kozhinov, A. N.; Gorshkov, M. V.; Tsybin, Y. O. On the Utility of Isotopic Fine Structure Mass Spectrometry in Protein Identification. *Anal. Chem.* **2012**, *84* (9), 4042−4051.
(27) Aizikov, K.; O'Connor, P. B. Use of the Filter Diagonalization Method in the Study of Space Charge Related Frequency Modulation in Fourier Transform Ion Cyclotron Resonance Mass Spectrometry. *J. Am. Soc. Mass Spectrom.* **2006**, *17* (6), 836−843.
(28) Aizikov, K.; Mathur, R.; O'Connor, P. B. The Spontaneous Loss of Coherence Catastrophe in Fourier Transform Ion Cyclotron Resonance Mass Spectrometry. *J. Am. Soc. Mass Spectrom.* **2009**, *20* (2), 247−256.
(29) Chen, S. P.; Comisarow, M. B. Modelling Coulomb Effects in Fourier-Transform Ion Cyclotron Resonance Mass Spectrometry by Charged Disks and Charged Cylinders. *Rapid Commun. Mass Spectrom.* **1992**, *6* (1), 1−3.
(30) Chen, S. P.; Comisarow, M. B. Simple Physical Models for Coulomb-Induced Frequency-Shifts and Coulomb-Induced Inhomogeneous Broadening for Like and Unlike Ions in Fourier-Transform Ion-Cyclotron Resonance Mass-Spectrometry. *Rapid Commun. Mass Spectrom.* **1991**, *5* (10), 450−455.
(31) Hofmann, A. E.; Chimiak, L.; Dallas, B.; Griep-Raming, J.; Juchelka, D.; Makarov, A.; Schwieters, J.; Eiler, J. M. Using Orbitrap Mass Spectrometry to Assess the Isotopic Compositions of Individual Compounds in Mixtures. *Int. J. Mass Spectrom.* **2020**, *457*, 116410.
(32) Qi, Y.; Witt, M.; Jertz, R.; Baykut, G.; Barrow, M. P.; Nikolaev, E. N.; O'Connor, P. B. Absorption-Mode Spectra on the Dynamically Harmonized Fourier Transform Ion Cyclotron Resonance Cell. *Rapid Commun. Mass Spectrom.* **2012**, *26* (17), 2021−2026.
(33) Tiquet, M.; La Rocca, R.; Kirnbauer, S.; Zoratto, S.; Van Kruining, D.; Quinton, L.; Eppe, G.; Martinez-Martinez, P.; Marchetti-Deschmann, M.; De Pauw, E.; Far, J. Ft-Icr Mass Spectrometry Imaging at Extreme Mass Resolving Power Using a Dynamically Harmonized Icr Cell with 1ω or 2ω Detection. *Anal. Chem.* **2022**, DOI: 10.1021/acs.analchem.2c00754.
(34) Schweihard, L.; Lindinger, M.; Kluge, H. J. Quadrupole-Detection Ft-Icr Mass Spectrometry. *Int. J. Mass Spectrom. Ion Processes* **1990**, *98* (1), 25−33.

https://doi.org/10.1021/jasms.2c00093
J. Am. Soc. Mass Spectrom. 2022, 33, 1499−1509

analytical chemistry

pubs.acs.org/ac
Article

Top-Down Proteoform Analysis by 2D MS with Quadrupolar Detection

Marek Polák, Michael Palasser, Alan Kádek, Daniel Kavan, Christopher A. Wootton, Marc-André Delsuc, Kathrin Breuker, Petr Novák,* and Maria A. van Agthoven*

Cite This: https://doi.org/10.1021/acs.analchem.3c02225

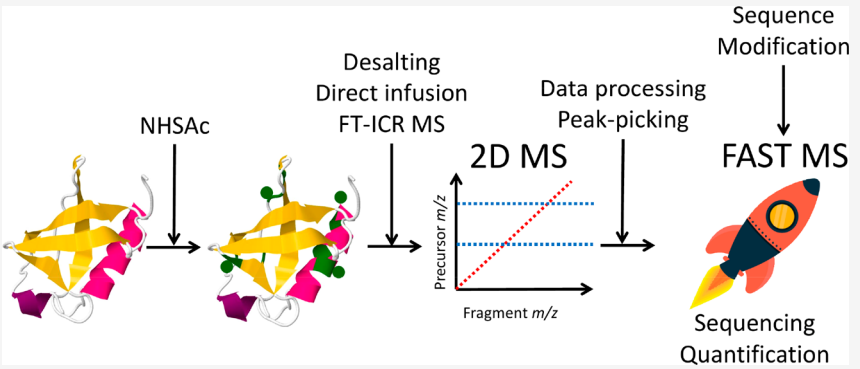

ABSTRACT: Two-dimensional mass spectrometry (2D MS) is a multiplexed tandem mass spectrometry method that does not rely on ion isolation to correlate the precursor and fragment ions. On a Fourier transform ion cyclotron resonance mass spectrometer (FT-ICR MS), 2D MS instead uses the modulation of precursor ion radii inside the ICR cell before fragmentation and yields 2D mass spectra that show the fragmentation patterns of all the analytes. In this study, we perform 2D MS for the first time with quadrupolar detection in a dynamically harmonized ICR cell. We discuss the advantages of quadrupolar detection in 2D MS and how we adapted existing data processing techniques for accurate frequency-to-mass conversion. We apply 2D MS with quadrupolar detection to the top-down analysis of covalently labeled ubiquitin with ECD fragmentation, and we develop a workflow for label-free relative quantification of biomolecule isoforms in 2D MS.

INTRODUCTION

In mass spectrometry (MS)-based structural analysis of biomolecules, there are multiple methods available to probe three-dimensional structures: noncovalent labeling such as hydrogen−deuterium exchange, radical or oxidative footprinting (for example, fast photochemical oxidation of proteins), amino acid- or base-selective probes, and chemical cross-linking.[1−6] The MS analysis of labeled biomolecules is performed by either a bottom-up or a top-down approach.[7−9]

High-resolution mass analyzers such as the Orbitrap or Fourier transform ion cyclotron resonance mass spectrometers (FT-ICR MS) enable the top-down tandem mass analysis of large biomolecules with complex fragmentation patterns.[10] The development of fragmentation methods that result in high sequence coverage and favor backbone fragmentation, such as electron capture dissociation (ECD) or ultraviolet photodissociation (UVPD), increases the accuracy of the location of the modifications induced by the chemical probing method.[11,12] Choosing top-down over bottom-up analysis reduces the number of experimental steps and the risk of losing the labels introduced by the probing methods.[13]

Nevertheless, top-down analysis comes with its own set of limitations. Because of the complexity and number of accessible dissociation pathways, ECD and UVPD often yield low-abundance fragments. As a result, they usually require the accumulation of approximately 10−100 measurements to obtain a satisfactory signal-to-noise ratio (SNR).[14,15] ECD and UVPD are therefore difficult fragmentation methods to couple with liquid chromatography (LC), which does not allow for the accumulation of much more than 10 scans for each analyte because of the rate of change of elution profile, even when using very fast and relatively low-resolution individual measurements.[12] In addition, standard tandem mass spectrometry techniques require the isolation of a single ion species to enable correlation between the precursor and

Received: May 23, 2023
Revised: September 26, 2023
Accepted: October 4, 2023

fragment ions, most often with a quadrupole mass filter.[16] This method of isolation creates a competition between the accuracy of the isolation and precursor ion abundances. The method also depends on the analytes of interest, thereby making data-independent acquisition difficult.[17,18] Moreover, for the analysis of protein modifications, no quadrupole-based isolation can separate overlapping isotopic distributions, although adding an ion mobility step has shown advantages.[19,20] Separation between isobaric ion species and coeluting species is therefore a limitation that all existing data-independent acquisition methods have in common.[21]

Two-dimensional mass spectrometry (2D MS) is a data-independent method for tandem mass spectrometry that does not require ion isolation or separation before fragmentation to correlate between precursor and fragment ions.[22] In a 2D FT-ICR MS experiment, ion radii are modulated in the ICR cell according to their cyclotron frequencies (which are inversely proportional to their mass-to-charge ratios, or m/z) before fragmentation with a radius-dependent fragmentation method such as infrared multiphoton dissociation (IRMPD), ECD, or UVPD.[23,24] The resulting fragment ion abundances (and therefore intensities) are modulated according to the cyclotron frequencies of the precursor ions.[25] The data set acquired in 2D MS experiments can be Fourier transformed to yield a two-dimensional mass spectrum (2D mass spectrum) that shows the fragmentation pattern of each precursor ion species analyzed in the ICR cell.[24]

2D MS has been applied to the analysis of small molecules, agrochemicals, polymers, and protein tryptic digests and the top-down analysis of proteins.[26−29] 2D MS has also been used for the label-free relative quantification of modified peptides in a proof-of-concept study.[30−32] One application of label-free quantification by 2D MS is the top-down analysis of covalently labeled proteins.

New developments in ICR cells have enabled increased resolving power and SNR in FT-ICR MS, which have improved top-down approaches for protein footprinting techniques.[7,33] In mass spectrometers equipped with dynamically harmonized ICR cells, quadrupolar 2ω detection can be optimized with the appropriate electronics. By detecting ion signals at the 2ω harmonic, the resolving power can be doubled for a given transient length or the transient length can be halved for a given resolving power-.[34] In this study, we perform 2D MS for the first time on a dynamically harmonized ICR cell with quadrupolar detection to determine the protein's solvent-accessible surface area. We then compare our results with a previously published study performed using standard tandem mass spectrometry on FT-ICR MS by isolating the $[M + 10H]^{10+}$ charge state of ubiquitin with increasing concentration of an acetylation reagent and fragmenting the ions by collision-induced dissociation (CID).[35]

In this study, we discuss the benefits of quadrupolar 2ω detection in 2D MS and our adapted data processing pipelines for the analysis of different proteoforms. We acetylated ubiquitin with a fivefold molar excess of *N*-hydroxysuccinimidyl acetate (NHSAc), and reaction products were analyzed with top-down 2D MS with ECD fragmentation. We show how 2D MS can be used for the analysis of the covalently labeled protein and what analytical information can be gleaned from 2D MS that cannot be obtained by isolating precursor ions before fragmentation.

EXPERIMENTAL METHODS

Sample Preparation. The acetylation of ubiquitin (50 μg) was achieved by diluting the sample in 50 mM triethylamine/bicarbonate (pH 7.6, Sigma-Aldrich, Saint Louis, MO) buffer at 0.5 mg/mL and adding the solution to a fivefold molar excess of NHSAc (Tokyo Chemical Industry Co Ltd., Tokyo, Japan) at room temperature for 1 h. The sample was desalted on an OPTI-TRAP macrotrap column (Optimize Technologies, Oregon City, OR) using an aqueous solution with 0.1% formic acid and eluted using an 80% acetonitrile/20% water solution with 0.1% formic acid. The solution was diluted to a 2 μM final protein concentration in aqueous solution of 1% acetic acid and 50% methanol for analysis (all solvents were LC-MS grade and obtained from Merck, Darmstadt, Germany).

Instrument Parameters. All experiments were performed on a 12 T solariX FT-ICR mass spectrometer (Bruker Daltonik, Bremen, Germany) with an electrospray ion source operated in positive mode and direct infusion at a flow rate of 108 μL/h.[36] Ions were accumulated for 0.5 s before being transferred to the dynamically harmonized ICR cell (2XR Paracell). The one-dimensional mass spectrum was acquired over an m/z range of 196.51−3000 in quadrupolar detection mode at the 2ω harmonic as described by Nikolaev *et al.*, with a 1 M data point transient with 64 averaged scans.[37,38]

The pulse sequence for the 2D MS experiment is shown in Scheme 1. The two pulses in the encoding sequence (precursor

Scheme 1. Pulse Sequence for the 2D MS Experiment with Frequency and m/z Range for Quadrupolar Detection[a]

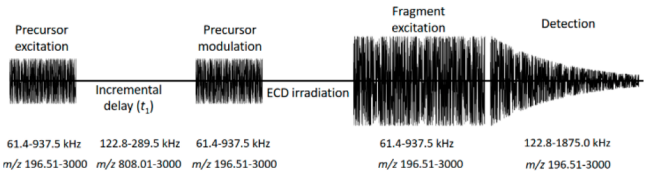

[a]Dimensions are not to scale.

detection and modulation) were set at 5.02 dB attenuation with 1.0 μs per excitation frequency step (frequency decrements were 625 Hz). The corresponding amplitude was estimated at 250 V_{pp}, with a 1.9% sweep excitation power for an amplifier with a maximum output of 446 V_{pp}. The encoding delay t_1 was increased 4096 times with a 3 μs increment, which corresponds to a 166.67 kHz frequency range. No phase-cycled signal averaging was employed in the experiment. Because of the digital clock in the Bruker electronics in quadrupolar 2ω detection, the minimum cyclotron frequency for the modulated precursor ions was 122.8 kHz for a maximum m/z of 3000 during excitation, leading to a m/z 808.1−3000 mass range for precursor ions. Captured ions were fragmented by ECD using the following parameters: the hollow cathode current was 1.3 A, the ECD pulse length 10 ms, the ECD lens 7 V, and the ECD bias 1.0 V.[39] Finally, in the horizontal fragment ion dimension, the excitation pulse in the detection sequence was set at 2.60 dB attenuation with a 15 μs/frequency step (frequency decrements were 625 Hz). The corresponding amplitude was estimated at 330 V_{pp}, with a 37% sweep excitation power for an amplifier with a maximum output of 446 V_{pp}. The horizontal mass range was m/z 196.51−3000 (corresponding to a frequency range of 1875.0−122.8 kHz). Transients were acquired over 0.559 s with 1

https://doi.org/10.1021/acs.analchem.3c02225
Anal. Chem. XXXX, XXX, XXX−XXX

million data points. The total duration of the experiment was 68 min.

Data Processing. The two-dimensional mass spectrum was processed and visualized using the Spectrometry Processing Innovative Kernel (SPIKE) software (available at www.github.com/spike-project, version 0.99.27, accessed on June 1, 2021) developed by the University of Strasbourg (Strasbourg, France) and CASC4DE (Illkirch-Graffenstaden, France) in the 64-bit Python 3.7 programming language on an open-source platform distributed by the Python Software Foundation (Beaverton, OR).[40] Processed data files were saved using the HDF5 file format. The 2D mass spectrum was apodized with the Kaiser apodization, zerofilled once, denoised with the SANE algorithm (with a rank of 30), and visualized in magnitude mode.[41] The size of the resulting data sets was 1 048 576 data points horizontally (fragment ion dimension) by 4096 data points vertically (precursor ion dimension).

Frequency-to-mass conversion was quadratic in both the vertical precursor ion dimension and the horizontal fragment ion dimension.[42] However, due to the quadrupolar 2ω detection, the parameters of the conversion equation were specific to each dimension, as will be discussed in the next section.[34] For each precursor ion species, five fragment ion scans were added up to cover the entire precursor isotopic distribution and obtain complete isotopic distributions for all fragment ions. The resulting one-dimensional fragment ion patterns were peak-picked in SPIKE. Peak assignments were performed using the Free Analysis Software for Top-down Mass Spectrometry (FAST-MS) developed by the University of Innsbruck (Innsbruck, Austria) in the 64-bit Python 3.7 programming language.[43] FAST-MS generated theoretical c/z and y fragment lists for ubiquitin variably modified with 4−6 acetylations located on lysine and methionine residues.

RESULTS AND DISCUSSION

In this study, the 2D MS experiment is performed in a dynamically harmonized ICR cell with quadrupolar 2ω four-plate detection.[34,44] The ICR cell was "shimmed" to ensure that the precursor ions were centered at the start of the pulse sequence (see Scheme 1).[38] The frequency range of the broadband pulses for precursor ion excitation and modulation covers the reduced cyclotron frequencies of the precursor and fragment ions (61.4−937.5 kHz). The frequencies measured during the transient cover the second harmonic of the reduced cyclotron frequencies of the precursor and fragment ions (122.8−1875.0 kHz). In addition, the digital modulation frequency was set by the instrument at twice the frequency of the highest m/z in the excitation pulse, instead of its cyclotron frequency as in detection of the fundamental frequencies.[24]

The first consequence of using quadrupolar detection is that, for an equivalent resolution and m/z range, each transient duration is halved, resulting in 2D MS experiments that are less time- and sample-consuming. The resolving power in the horizontal fragment ion dimension remains theoretically unchanged, while the SNR in quadrupolar 2ω detection is typically reduced compared to that in standard detection.[45,46] Second, the coefficients required in the frequency-to-mass conversion equation of 2D mass spectra recorded with quadrupolar 2ω detection are doubled in the horizontal fragment ion dimension compared to the coefficients for the frequency-to-mass conversion in the vertical fragment ion dimension. Finally, the digital modulation frequency set by the instrument electronics is doubled in quadrupolar 2ω detection compared to that in the detection of the fundamental frequencies (see Scheme 1).The modulation frequency for a precursor ion is defined as $f_{ICR} - f_{min}$, where f_{ICR} is the reduced cyclotron frequency of the ion and f_{min} is the digital modulation frequency set by the instrument electronics. Doubling f_{min} increases the lowest precursor m/z, which corresponds to a cyclotron frequency of $f_N + f_{min}$, where f_N is the Nyquist frequency or reduces the necessary Nyquist frequency.[22] In the 2D MS experiment, the Nyquist frequency in the vertical dimension corresponds to the cyclotron frequency range of the precursor ions. With all other parameters remaining equal, reducing the frequency range increases the theoretical resolving power of the 2D mass spectrum in the vertical dimension.[30]

Figure 1a displays the 2D ECD mass spectrum of acetylated ubiquitin. Fragment m/z values are plotted horizontally, and precursor m/z values are plotted vertically. The autocorrelation line $(m/z)_{precursor} = (m/z)_{fragment}$ (i.e., identity line) results from the modulation of precursor ion radii and abundances with their own reduced cyclotron frequencies and shows all the precursor ions observed in the 2D MS analysis. Horizontally, fragment ion scans show the fragmentation pattern of each precursor ion. Vertically, precursor ion scans show all the

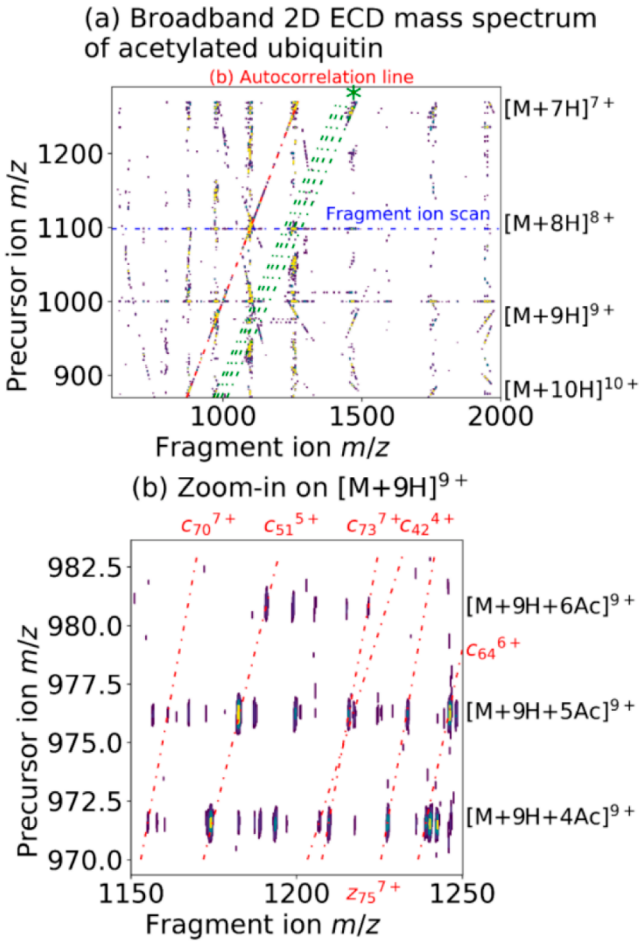

Figure 1. (a) 2D ECD mass spectrum of acetylated ubiquitin. An asterisk (*) indicates electron capture lines (green). (b) Zoom-in on the fragmentation pattern of $[M + H]^{9+}$ with 4−6 acetylations. The red lines indicate dissociation lines for the various c and z fragments listed around the periphery.

https://doi.org/10.1021/acs.analchem.3c02225
Anal. Chem. XXXX, XXX, XXX−XXX

precursors of a given fragment ion. The horizontal resolving power ($m/\Delta m$, where Δm is the full-width at half-maximum of the fragment ion peak) was measured to be 200 000 at m/z 400 and the vertical resolving power was 1300 at m/z 874 (corresponding to 2800 at m/z 400). We can also extract electron capture lines as follows:

$$[M + nH]^{n+} + e^- \rightarrow [M + nH]^{(n-1)+\bullet} \quad (1)$$

$$(m/z)_{\text{precursor}} = \frac{n-1}{n}(m/z)_{\text{fragment}} \quad (2)$$

where n is the charge state of the precursor ions. In Figure 1a, electron capture lines for the capture of one electron by the 7−10+ charge states are plotted in green. As shown in eq 2, their slopes are 6/7, 7/8, 8/9, and 9/10.

The 2D ECD mass spectrum also shows harmonics of the autocorrelation line as curved lines. The presence of harmonic peaks is caused by the nonsinusoidal modulation of the precursor ions.[22,25] Scintillation noise, which is caused by the fluctuation of the number of ions in the ICR cell from scan to scan, manifests as vertical streaks along the m/z of the precursor ions and can be filtered out by the use of a denoising algorithm during data processing.[41] Figure S1 in the Supporting Information shows the complete 2D mass spectrum, including harmonics of the autocorrelation line. Most harmonics are similar to the ones obtained in 2D MS with standard detection at 1ω. One noticeable difference between detection at 1ω and quadrupolar detection at 2ω is the presence of the 1ω subharmonic frequency (at double the measured m/z). In the 2D mass spectrum, we observe the subharmonic peak of the autocorrelation line at a 1/2 slope at approximately 15−20% the intensity of the autocorrelation line.[24]

Here, the 2D mass spectrum is shown as a contour plot, but we cannot see enough detail to show the fragmentation patterns of the 7−10+ charge states of acetylated ubiquitin. Because of the multiplicity of dissociation channels for the fragmentation of proteins in ECD, relative intensities of fragment ions in the 2D mass spectrum can be equivalent to the intensity of signals caused by harmonics or noise, and plotting one without the other is difficult.[47] Nevertheless, discriminating analytically useful signal from noise is readily achieved because, due to distinctly different frequency relationships, they are in different areas of the spectrum. The zoomed-in view of the fragmentation patterns shown in Figure 1b illustrates how the fragmentation patterns can be easily distinguished. The red lines highlight various dissociation lines to illustrate how they can be used to locate modifications.

Figure 2a shows the extracted autocorrelation line (m/z 850−1300) of the 2D ECD mass spectrum. The charge states of acetylated ubiquitin that are modulated and fragmented in this 2D mass spectrum are 7−10+, each of them bearing 4−6 acetylations, which is consistent with the level of acetylation under similar labeling conditions presented by Novák *et al.*[35] The inset shows the isotopic distribution of the $[M + 10H + 4Ac]^{10+}$ precursor ion species on the autocorrelation line. The signal from precursor ions is modulated by the radius (during the pulse-delay-pulse sequence in Scheme 1) and by their abundance (during the ECD irradiation), followed by Fourier transformation over 4096 scans. Therefore, the SNR on the autocorrelation line is typically very high.[48] In the case of the isotopic distribution of $[M + 10H + 4Ac]^{10+}$, the SNR for the most intense peak is 720. The SNR for the monoisotopic peak

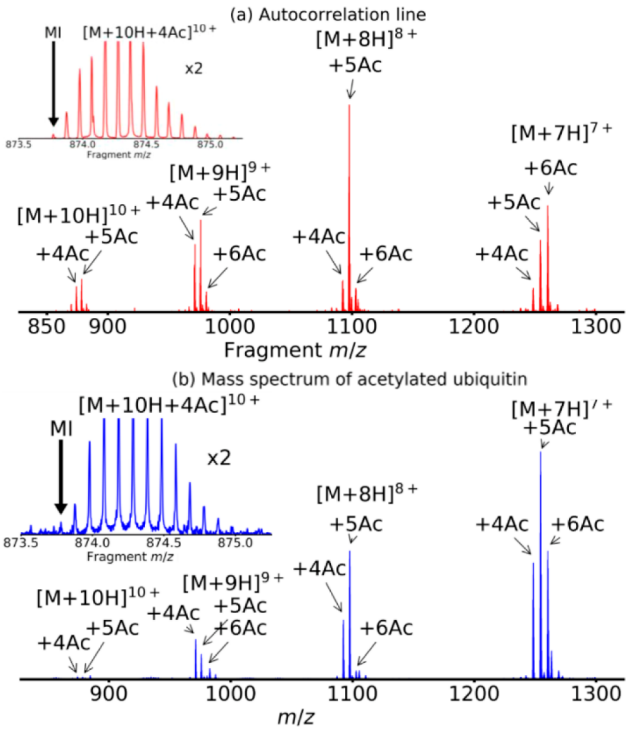

Figure 2. (a) Extracted autocorrelation line from the 2D mass spectrum. The inset shows a zoomed-in view of the isotopic distribution of the $[M + 10H + 4Ac]^{10+}$. The arrow marks the monoisotopic peak (MI). (b) Mass spectrum of acetylated ubiquitin. The inset shows the zoomed-in isotopic distribution of the $[M + 10H + 4Ac]^{10+}$ species from the mass spectrum shown in Figure 2b. The arrow marks the monoisotopic peak (MI).

is 20. For comparison, Figure 2b shows the 1D mass spectrum of acetylated ubiquitin. Both the mass spectrum and the autocorrelation line show similar charge state ranges and acetylation numbers for each charge state. However, the relative intensities of the peaks are different between Figure 2a and Figure 2b: while the relative intensities in the mass spectrum reflect ion abundance and charge state, the relative intensities on the autocorrelation line also reflect the fragmentation efficiency of each ion species, which, for ECD, depends greatly on charge state.[24,49] The SNR for the monoisotopic peak of $[M + 10H + 4Ac]^{10+}$ in the mass spectrum is only 2−3, which is about 10× smaller than that for the same monoisotopic peak extracted from the autocorrelation line in Figure 2a. With 4096 scans instead of 64, the SNR would be 8× higher.

One issue in the top-down analysis of large biomolecules is their accurate mass determination. Typically, deconvolution algorithms based on the averagine method are used because the SNR of the monoisotopic peak is often below the level of detection.[50] Although most biomolecules for which this issue arises are much larger than ubiquitin, this result suggests that using the autocorrelation line in 2D mass spectra may offer more accurate analytical information by offering higher SNRs for monoisotopic peaks of biomolecules. The process of peak assignment and sequence coverage determination using FAST-MS is illustrated in Figure 3 for each ubiquitin isoform. Figure 3a shows the summed fragment ion scans of m/z 1098 ($[M + 8H + 5Ac]^{8+}$). Five fragment ion scans were extracted from the 2D mass spectrum to cover the precursor ion peak of $[M + 8H + 5Ac]^{8+}$ at m/z 1098 and co-added to obtain the resulting

https://doi.org/10.1021/acs.analchem.3c02225
Anal. Chem. XXXX, XXX, XXX−XXX

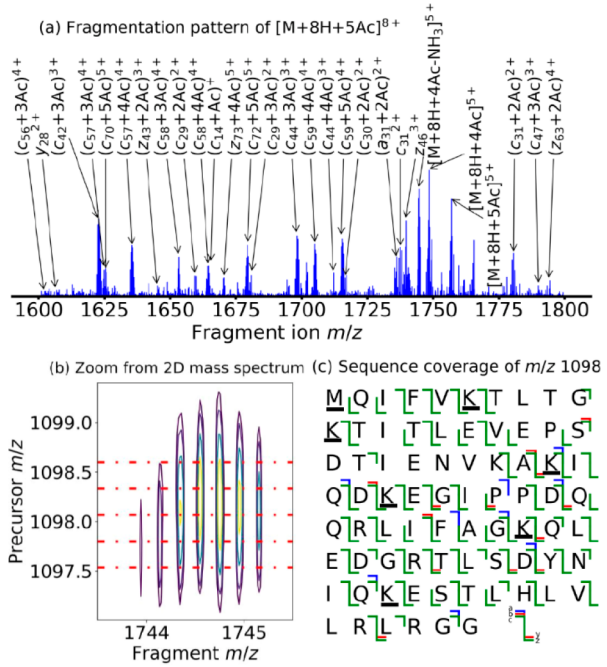

Figure 3. (a) Added-up fragment ion scans of m/z 1098 ($[M + 8H + 5Ac]^{8+}$) extracted from the 2D mass spectrum of acetylated ubiquitin. (b) Zoom-in on the isotopic distribution of $[M + 8H + 4Ac - NH_3]^{5+}$ from the $[M + 8H + 5Ac]^{8+}$ precursor, with lines marking the fragment ion scans added up to obtain Figure 2a. (c) Sequence coverage of $[M + 8H + 5Ac]^{8+}$, totaling 86% (acetylated residues underlined).

fragment ion scan shown in Figure 3a. In Figure 3b, we illustrate why the fragment ion scans were added up (individual extracted scans are shown in red). Since the resolving power in the vertical precursor ion dimension is insufficient to distinguish between precursor ion isotopes, the overlap between precursor ion isotopic peaks is not complete. The relative intensities in fragment ion isotopic distributions in a single fragment ion scan can therefore be distorted; to recover the full isotopic distribution for fragment ions, we summed up the fragment ion scans before analysis. FAST-MS compares experimental and theoretical relative intensities to gauge the quality of peak assignments, peak-picking the fragmentation pattern for the full isotopic distribution of each protein isoform, then improves the accuracy of the sequence coverage assignment, which provides an optional advantage of adding-up adjacent scans in 2D MS. Because the fragment ion scans are adjacent, noise signals are correlated between them and the SNR is only marginally affected.

The information fed into FAST-MS was the ubiquitin sequence, the molecular formula of the acetylation, the number of modifications, and the location of the modification (M and K residues). The software then generated a library of theoretical isotopic distributions of the *a*, *b*, *c*, *y*, and *z* fragments. Figure 3c shows the sequence coverage of $[M + 8H + 5Ac]^{8+}$. All peak assignments were validated manually, reaching a sequence coverage of 86%. For comparison, a one-dimensional tandem mass spectrum of $[M + 8H + (0-6)Ac]^{8+}$ in similar conditions with 2 M data points and 200 accumulated scans yielded a cleavage coverage of 84% (see Table S12 and Figure S2 in the Supporting Information).

The lists of peak assignments can be found in Tables S1–S11 in the Supporting Information. Table 1 summarizes the

Table 1. Sequence Coverage of Each Precursor Ion in the 2D Mass Spectrum of Acetylated Ubiquitin[a]

	$[M + 10H]^{10+}$	$[M + 9H]^{9+}$	$[M + 8H]^{8+}$	$[M + 7H]^{7+}$	total
+4Ac	34%	63%	36%	16%	84%
+5Ac	57%	67%	86%	46%	89%
+6Ac	N/A	32%	30%	34%	60%

[a]Legend: Ac = acetylation, N/A = not annotated.

sequence coverage for each proteoform and charge state of acetylated ubiquitin. Each fragmentation pattern has a different sequence coverage, which depends on both the abundance of each precursor ion and charge state because the fragmentation efficiency of ECD is charge state-dependent.[11] The last column shows the sequence coverage for each ubiquitin proteoform after the results for all charge states. Because different fragments are produced for each charge state, the total sequence coverage is higher than the sequence coverage of each charge state.

Figure 4 shows the acetylation rate vs the residue index for proteoforms with four, five, and six acetylations, for *c* and *z* fragments. Each plot combines the peak assignments for all charge states (7–10+) with M/K acetylation sites assigned by FAST-MS. These plots allow us to locate acetylation sites and quantify the extent of acetylation.[30−32]

Figure 4a shows the extent of acetylation for ubiquitin with four acetylations from *c* fragments and *z* fragment ions, respectively. Ubiquitin has eight possible acetylation sites, namely, M1, K6, K11, K27, K29, K33, K48, and K63. From the N-terminus, the acetylation sites are M1, K6, K48, and K63. From the C-terminus, the acetylation sites are K63, K48, K33, and K6. The most easily accessible sites can therefore be located at K63, K48, and K6. Residues M1, K11, K27, K29, and K33 are less solvent-accessible. The sequence coverage for ubiquitin with four acetylations is not sufficient to distinguish between K27, K29, and K33.

Figure 4b shows the acetylation rate for ubiquitin with five acetylations from *c* and *z* fragments, respectively. From the N-terminus, the acetylation sites are M1, K6, K29/33, K48, and K63. From the C-terminus, the acetylation sites are K63, K48, K33, K11, and K6 or M1. Figure 4c shows the acetylation rate for ubiquitin with six acetylations from *c* fragments and *z* fragments, respectively. From the N-terminus, the acetylation sites are M1, K6, K11, K29, K48, and K63. From the C-terminus, the acetylation sites are K63, K48, K33, K27, K11, and M1.

From these results, we can conclude that the most accessible acetylation sites are K63 and K48; followed by K6, M1, and K33; and finally K29, K27, and K11. This conclusion is congruent with the conclusions by top-down CID MS/MS found by Novák *et al.*[35] We should note that we observe a loss of acetylation in Figure 3a. However, despite this result, all acetylation sites for each isoform could be accounted for.

One advantage of broadband-mode 2D MS over individual MS/MS spectra is the ease with which the interactions between the charge state and protein modifications can be measured. Since lysine, which is the main residue carrying the acetylation, also carries the charge, and since acetylation is known for reducing positive charges in proteins, we hypothesized that the charge state of ubiquitin would be affected by acetylation.[51] We calculated the average charge state of ubiquitin for each number of acetylations using the intensities on the autocorrelation line and the mass spectrum.

https://doi.org/10.1021/acs.analchem.3c02225
Anal. Chem. XXXX, XXX, XXX−XXX

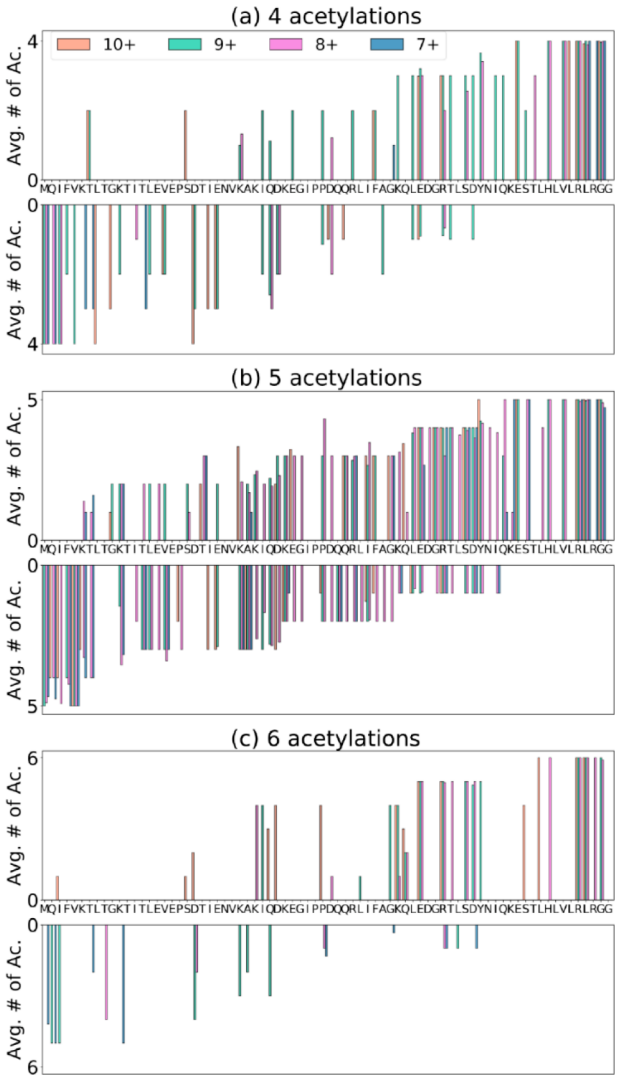

Figure 4. Acetylation rate vs residue index for ubiquitin modified with (a) four acetylations (c fragments on top, z fragments at the bottom), (b) five acetylations (c fragments on top, z fragments at the bottom), and (c) six acetylations (c fragments on top, z fragments at the bottom).

Since measured intensities in FT-ICR MS are proportional to the abundance and the charge of each ion species, we calculated the average charge state for each proteoform using the following equation:

$$\langle z \rangle(n) = \frac{\sum_z I(z, n)}{\sum_z (I(z, n)/z)} \tag{3}$$

where $\langle z \rangle(n)$ is the average charge state for n acetylations and $I(z, n)$ is the intensity of the $[M + zH + nAc]^{z+}$ peaks.

The results are plotted in figure S3 in the Supporting Information. The average charge state decreases with the number of acetylations, both in the mass spectrum and in the autocorrelation line, which is consistent with acetylation reducing the number of positive charges on a protein. The results also show that the average charge state is higher in the autocorrelation line than in the mass spectrum, which is due to factors determining the intensity of a peak in FT-ICR MS. In the mass spectrum, peak intensities are determined by the ion abundance and the charge state. On the autocorrelation line of a 2D ECD mass spectrum, peak intensities are determined by the ion abundance, the charge state and the capacity to capture electrons, which increases with charge state in positive ionization mode.[24] Therefore, the average charge state for each isoform is higher in the autocorrelation line of the 2D mass spectrum than in the 1D mass spectrum.

In Figure 5, we seek to determine whether the acetylation of both lysine and N-terminus methionine reduces the charge

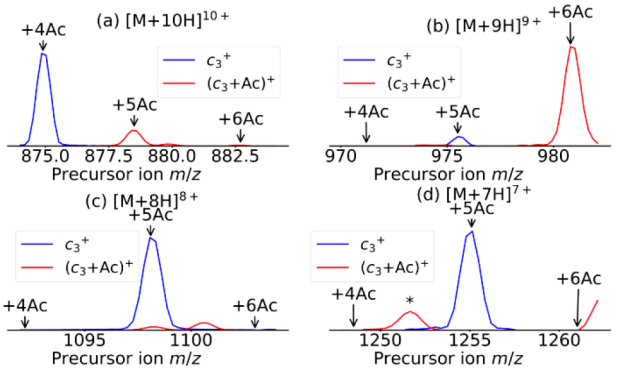

Figure 5. Precursor ion scans for c_3 (m/z 390.21790, blue) and c_3 + Ac (m/z 432.22714, red) fragments for (a) 10+, (b) 9+, (c) 8+, and (d) 7+ precursor charge states. An asterisk (*) indicates an artifact caused by the denoising algorithm.

state of ubiquitin. Therefore, we extracted the vertical precursor ion scans from the 2D mass spectrum for the c_3 (m/z 390.21790, blue) and c_3+Ac (m/z 432.22714, red) fragments, which, in turn, enables us to quantify the acetylation of only the M1 residue in ubiquitin. Figure 5 shows the c_3 fragment ion (blue) alongside with its acetylated form (c_3 + Ac, red) for charge states 10−7+ in Figure 5a−d, respectively.

Figure 5a shows that ubiquitin with four acetylations produces the c_3 fragment and that ubiquitin with five and six acetylations produce the c_3 + Ac fragment in the 10+ charge state. Therefore, the fifth most favored acetylation site is M1. In Figure 5b, for 9+ charged precursors, the c_3 + Ac fragment is only produced from the ubiquitin with six acetylations, which means that M1 is the sixth most favored acetylation site. In Figure 5c and d, we see that only c_3 is produced from the 7+ and 8+ charge states, which means that M1 is, at best, the seventh most favored acetylation site. As a result, we can say that ubiquitin with an acetylation on the M1 residue skews toward higher charge states. This result suggests that the acetylation of the methionine residue may not reduce the charge state of ubiquitin like the acetylation of the lysine residues does.

CONCLUSION

Stable protein covalent labeling coupled to 2D MS analysis and ECD fragmentation has yielded information about solvent accessibility at individual residues, particularly the N-terminus methionine and the lysines residues.[35] For the first time, 2D MS was applied with quadrupolar detection on a dynamically harmonized ICR cell. The detection at the 2ω harmonic led to a shorter experimental duration and an increase in resolving power in the vertical precursor ion dimension.[34]

Because of the multiplexing inherent to the 2D MS experiment, we were able to obtain in parallel the ECD fragmentation pattern of four charge states of ubiquitin with up to six acetylations each.[24] The resolving power in the vertical

https://doi.org/10.1021/acs.analchem.3c02225
Anal. Chem. XXXX, XXX, XXX−XXX

precursor ion scan was sufficient to confidently correlate precursor and fragment ions without unwanted contributions from different proteoforms and without a loss of precursor ion abundance due to quadrupole isolation. We used the FAST-MS software and defined a workflow to assign all fragment ions generated from each charge state by ECD and quantify the extent of acetylation of methionine/lysine residues, which was consistent with previously published results.[30,4335]

2D MS showed the advantages of having the fragmentation patterns of multiple isoforms and charge states in a single spectrum. First, the sequence coverage from the combined fragmentation patterns of all observed charge states was higher than the sequence coverage obtained from the charge state with the highest fragmentation efficiency. Second, the 2D mass spectrum enabled the observation that acetylation reduces the gas-phase charge state of ubiquitin and more specifically that the acetylation of lysine residues reduces the charge state to a higher degree than the acetylation of the N-terminus M1 residue.

This study shows the potential for 2D MS coupled with ECD fragmentation to yield comprehensive analytical information for the top-down analysis of the proteoform mixtures. 2D ECD MS can further be applied to the quantitative analysis of post-translational modifications of proteins and to the structural analysis of covalently labeled proteins.

■ ASSOCIATED CONTENT

Data Availability Statement

Raw data and processing parameter file available at https://zenodo.org/uploads/10027010.

Supporting Information

The Supporting Information is available free of charge at https://pubs.acs.org/doi/10.1021/acs.analchem.3c02225.

Peaklists and assignments for the extracted fragment ion scans from the 2D mass spectrum and the tandem mass spectrum, full 2D mass spectrum, and plot of the average charge state of each proteoform (PDF)

■ AUTHOR INFORMATION

Corresponding Authors

Petr Novák − *Institute of Microbiology of the Czech Academy of Sciences, Prague 14220, Czech Republic; Faculty of Science, Charles University, Prague 12843, Czech Republic;* orcid.org/0000-0001-8688-529X; Email: pnovak@biomed.cas.cz

Maria A. van Agthoven − *Institute of Microbiology of the Czech Academy of Sciences, Prague 14220, Czech Republic; Center for Chemistry and Biomedicine, University of Innsbruck, 6020 Innsbruck, Austria;* Present Address: Université de Rouen, 1 rue Tesnière, 76821 Mont-Saint-Aignan, France; orcid.org/0000-0003-2438-3934; Email: maria.vanagthoven@biomed.cas.cz

Authors

Marek Polák − *Institute of Microbiology of the Czech Academy of Sciences, Prague 14220, Czech Republic; Faculty of Science, Charles University, Prague 12843, Czech Republic*

Michael Palasser − *Center for Chemistry and Biomedicine, University of Innsbruck, 6020 Innsbruck, Austria;* Present Address: Bachem AG, Hauptstrasse 144, 4416 Bubendorf, Switzerland

Alan Kádek − *Institute of Microbiology of the Czech Academy of Sciences, Prague 14220, Czech Republic*

Daniel Kavan − *Institute of Microbiology of the Czech Academy of Sciences, Prague 14220, Czech Republic; Faculty of Science, Charles University, Prague 12843, Czech Republic*

Christopher A. Wootton − *Bruker Daltonics GmbH & Co KG, 28359 Bremen, Germany*

Marc-André Delsuc − *Institut de Génétique et de Biologie Moléculaire et Cellulaire, INSERM, U596, CNRS, UMR7104, Université de Strasbourg, 67404 Illkirch-Graffenstaden, France;* orcid.org/0000-0002-1400-5326

Kathrin Breuker − *Center for Chemistry and Biomedicine, University of Innsbruck, 6020 Innsbruck, Austria;* orcid.org/0000-0002-4978-0883

Complete contact information is available at: https://pubs.acs.org/10.1021/acs.analchem.3c02225

Author Contributions

The manuscript was written through contributions of all authors. They have given approval to the final version of the manuscript

Funding

Open Access is funded by the Austrian Science Fund (FWF).

Notes

The authors declare no competing financial interest.

■ ACKNOWLEDGMENTS

The authors thank Dr. Petr Man, Dr. Petr Pompach, Dr. Zdeněk Kukačka, and Dr. Michael Volný for helpful discussions. This work was primarily supported by the European Commission H2020 (EU_FT-ICR_MS grant agreement ID 731077); the International Mobility of Researchers of the Institute of Microbiology of the CAS, v.v.i. no. 2 (CZ.02.2.69/0.0/0.0/18_053/0017705); and the Czech Science Foundation (22-27695S). Additional institutional and facility support from the Academy of Sciences of the Czech Republic (RVO 61388971), the Grant Agency of Charles University (project 359521), and the European Regional Development Funds (CZ.1.05/1.1.00/02.0109 BIOCEV) are gratefully acknowledged. M.P. and P.N. acknowledge funding through the NPO-NEURO-EXCELLES LX22NPO5107 project. M.v.A. and K.B. thank the Austrian Science Fund for the List Meitner Fellowship M2757-B. Supported by project no. LX22NPO5107 (MEYS) financed by European Union−Next Generation EU.

■ REFERENCES

(1) Fabris, D.; Yu, E. T. *J. Mass Spectrom.* **2010**, *45* (8), 841−860.

(2) Takamoto, K.; Chance, M. R. *Annu. Rev. Biophys. Biomol. Struct.* **2006**, *35* (1), 251−276.

(3) Sinz, A. *Mass Spectrom. Rev.* **2006**, *25* (4), 663−682.

(4) Fojtík, L.; Fiala, J.; Pompach, P.; Chmelík, J.; Matoušek, V.; Beier, P.; Kukačka, Z.; Novák, P. *J. Am. Chem. Soc.* **2021**, *143* (49), 20670−20679.

(5) Yan, X.; Maier, C. S. Hydrogen/Deuterium Exchange Mass Spectrometry. In *Mass Spectrometry of Proteins and Peptides: Methods and Protocols*, Lipton, M. S., Paša-Tolic, L., Eds.; Methods in Molecular Biology, Vol. *492*; Humana Press: Totowa, NJ, 2009; pp 255−271.

(6) Niu, B.; Gross, M. L. MS-Based Hydroxyl Radical Footprinting: Methodology and Application of Fast Photochemical Oxidation of Proteins (FPOP). In *Mass Spectrometry-Based Chemical Proteomics*;

Tao, W. A., Zhang, Y., Eds.; John Wiley & Sons, Inc.: New York, NY, 2019; pp 363−416.
(7) Polák, M.; Yassaghi, G.; Kavan, D.; Filandr, F.; Fiala, J.; Kukačka, Z.; Halada, P.; Loginov, D. S.; Novák, P. *Anal. Chem.* **2022**, *94* (7), 3203−3210.
(8) Chen, J.; Cui, W.; Giblin, D.; Gross, M. L. *J. Am. Chem. Soc.* **2012**, *23* (8), 1306−1318.
(9) Novak, P.; Young, M. M.; Schoeniger, J. S.; Kruppa, G. H. *Eur. J. Mass Spectrom.* **2003**, *9* (6), 623−631.
(10) Marshall, A. G.; Hendrickson, C. L. *Annu. Rev. Anal. Chem.* **2008**, *1*, 579−599.
(11) Zubarev, R. A.; Horn, D. M.; Fridriksson, E. K.; Kelleher, N. L.; Kruger, N. A.; Lewis, M. A.; Carpenter, B. K.; McLafferty, F. W. *Anal. Chem.* **2000**, *72* (3), 563−573.
(12) Cannon, J. R.; Cammarata, M. B.; Robotham, S. A.; Cotham, V. C.; Shaw, J. B.; Fellers, R. T.; Early, B. P.; Thomas, P. M.; Kelleher, N. L.; Brodbelt, J. S. *Anal. Chem.* **2014**, *86* (4), 2185−2192.
(13) Moradian, A.; Kalli, A.; Sweredoski, M. J.; Hess, S. *PROTEOMICS* **2014**, *14* (4−5), 489−497.
(14) Kruger, N. A.; Zubarev, R. A.; Carpenter, B. K.; Kelleher, N. L.; Horn, D. M.; McLafferty, F. W. *Int. J. Mass Spectrom.* **1999**, *182* (183), 1−5.
(15) Brodbelt, J. S.; Morrison, L. J.; Santos, I. *Chem. Rev.* **2020**, *120* (7), 3328−3380.
(16) Glish, G. L.; Burinsky, D. J. *J. Am. Soc. Mass Spectrom.* **2008**, *19* (2), 161−172.
(17) Douglas, D. J.; French, J. B. *J. Am. Soc. Mass Spectrom.* **1992**, *3* (4), 398−408.
(18) Wootton, C. A.; Lam, Y. P. Y.; Willetts, M.; van Agthoven, M. A.; Barrow, M. P.; Sadler, P. J.; O'Connor, P. B. *Analyst* **2017**, *142* (11), 2029−2037.
(19) Smith, D. F.; Blakney, G. T.; Beu, S. C.; Anderson, L. C.; Weisbrod, C. R.; Hendrickson, C. L. *Anal. Chem.* **2020**, *92* (4), 3213−3219.
(20) Wongkongkathep, P.; Han, J. Y.; Choi, T. S.; Yin, S.; Kim, H. I.; Loo, J. A. *J. Am. Soc. Mass Spectrom.* **2018**, *29* (9), 1870−1880.
(21) Zhang, F.; Ge, W.; Ruan, G.; Cai, X.; Guo, T. *PROTEOMICS* **2020**, *20* (17−18), 1900276.
(22) Pfändler, P.; Bodenhausen, G.; Rapin, J.; Walser, M. E.; Gäumann, T. *J. Am. Chem. Soc.* **1988**, *110* (17), 5625−5628.
(23) Marzullo, B. P.; Morgan, T. E.; Theisen, A.; Haris, A.; Wootton, C. A.; Perry, S. J.; Saeed, M.; Barrow, M. P.; O'Connor, P. B. *Anal. Chem.* **2021**, *93* (27), 9462−9470.
(24) van Agthoven, M. A.; Lam, Y. P. Y.; O'Connor, P. B.; Rolando, C.; Delsuc, M.-A. *Eur. Biophys. J.* **2019**, *48* (3), 213−229.
(25) Guan, S.; Jones, P. R. *J. Chem. Phys.* **1989**, *91* (9), 5291−5.
(26) Morgan, T. E.; Wootton, C. A.; Marzullo, B.; Paris, J.; Kerr, A.; Ellacott, S. H.; van Agthoven, M. A.; Barrow, M. P.; Bristow, A. W. T.; Perrier, S.; O'Connor, P. B. *J. Am. Soc. Mass Spectrom.* **2021**, *32* (8), 2153−2161.
(27) Floris, F.; van Agthoven, M.; Chiron, L.; Soulby, A. J.; Wootton, C. A.; Lam, Y. P. Y.; Barrow, M. P.; Delsuc, M.-A.; O'Connor, P. B. *J. Am. Soc. Mass Spectrom.* **2016**, *27* (9), 1531−1538.
(28) Marzullo, B. P.; Morgan, T. E.; Wootton, C. A.; Perry, S. J.; Saeed, M.; Barrow, M. P.; O'Connor, P. B. *Anal. Chem.* **2020**, *92* (17), 11687−11695.
(29) Paris, J.; Morgan, T. E.; Marzullo, B. P.; Wootton, C. A.; Barrow, M. P.; O'Hara, J.; O'Connor, P. B. *J. Am. Soc. Mass Spectrom.* **2021**, *32* (7), 1716−1724.
(30) Halper, M.; Delsuc, M.-A.; Breuker, K.; van Agthoven, M. A. *Anal. Chem.* **2020**, *92* (20), 13945−13952.
(31) Delsuc, M.-A.; Breuker, K.; van Agthoven, M. A. *Molecules* **2021**, *26* (11), 3388.
(32) Palasser, M.; Heel, S. V.; Delsuc, M.-A.; Breuker, K.; van Agthoven, M. A. *J. Am. Soc. Mass Spectrom.* **2023**, *34* (4), 608−616.
(33) Yassaghi, G.; Kukačka, Z.; Fiala, J.; Kavan, D.; Halada, P.; Volný, M.; Novák, P. *Anal. Chem.* **2022**, *94* (28), 9993−10002.
(34) Schweihard, L.; Lindinger, M.; Kluge, H.-J. *Int. J. Mass Spectrom. Ion Process.* **1990**, *98* (1), 25−33.
(35) Novak, P.; Kruppa, G. H.; Young, M. M.; Schoeniger, J. *J. Mass Spectrom.* **2004**, *39* (3), 322−328.
(36) Taucher, M.; Breuker, K. *J. Am. Soc. Mass Spectrom.* **2010**, *21* (6), 918−929.
(37) Schweikhard, L.; Lindinger, M.; Kluge, H. J. *Rev. Sci. Instrum.* **1990**, *61* (3), 1055−1058.
(38) Jertz, R.; Friedrich, J.; Kriete, C.; Nikolaev, E. N.; Baykut, G. *J. Am. Soc. Mass Spectrom.* **2015**, *26* (8), 1349−1366.
(39) Tsybin, Y. O.; Quinn, J. P.; Tsybin, O. Y.; Hendrickson, C. L.; Marshall, A. G. *J. Am. Soc. Mass Spectrom.* **2008**, *19* (6), 762−771.
(40) Chiron, L.; Coutouly, M.-A.; Starck, J.-P.; Rolando, C.; Delsuc, M.-A. *arXiv (Physics.Computational Physics)* **2016**, 1608.06777.
(41) Bray, F.; Bouclon, J.; Chiron, L.; Witt, M.; Delsuc, M.-A.; Rolando, C. *Anal. Chem.* **2017**, *89* (17), 8589−8593.
(42) Ledford, E. B., Jr.; Rempel, D. L.; Gross, M. L. *Anal. Chem.* **1984**, *56* (14), 2744−8.
(43) Palasser, M. *FAST-MS*. https://github.com/michael-palasser/FAST-MS (accessed 2022-01-07).
(44) Nikolaev, E. N.; Boldin, I. A.; Jertz, R.; Baykut, G. *J. Am. Soc. Mass Spectrom.* **2011**, *22* (7), 1125−1133.
(45) Driver, J. A.; Kharchenko, A.; Amster, I. J. *Int. J. Mass Spectrom.* **2020**, *455*, 116372.
(46) Wu, Q.; Gorshkov, M. V.; Paša-Tolić, L. *Int. J. Mass Spectrom.* **2021**, *469*, 116669.
(47) Cooper, H. J.; Hakansson, K.; Marshall, A. G. *Mass Spectrom. Rev.* **2005**, *24* (2), 201−222.
(48) Fellgett, P. B. *J. Opt. Soc. Am.* **1949**, *39*, 970−6.
(49) Marshall, A. G.; Hendrickson, C. L.; Jackson, G. S. *Mass Spectrom. Rev.* **1998**, *17* (1), 1−35.
(50) Valkenborg, D.; Jansen, I.; Burzykowski, T. *J. Am. Soc. Mass Spectrom.* **2008**, *19* (5), 703−712.
(51) Masuda, T.; Ide, N.; Kitabatake, N. *Chemical Senses* **2005**, *30* (3), 253−264.

https://doi.org/10.1021/acs.analchem.3c02225
Anal. Chem. XXXX, XXX, XXX−XXX